ERDC/CRREL TR-18-14

Cold Regions Research and Engineering Laboratory

US Army Corps of Engineers®
Engineer Research and Development Center

ERDC
ENGINEER RESEARCH & DEVELOPMENT CENTER

ERDC 6.2 Geospatial Research and Engineering (GRE) ARTEMIS STO-R GRAIL

Soil Strength Analysis of Sonoran Desert Landforms

Sally A. Shoop, Samuel A. Beal, Wendy L. Wieder, and Eric V. McDonald

August 2018

The U.S. Army Engineer Research and Development Center (ERDC) solves the nation's toughest engineering and environmental challenges. ERDC develops innovative solutions in civil and military engineering, geospatial sciences, water resources, and environmental sciences for the Army, the Department of Defense, civilian agencies, and our nation's public good. Find out more at www.erdc.usace.army.mil.

To search for other technical reports published by ERDC, visit the ERDC online library at http://acwc.sdp.sirsi.net/client/default.

ERDC/CRREL TR-18-14
August 2018

Soil Strength Analysis of Sonoran Desert Landforms

Sally A. Shoop, Samuel A. Beal, and Wendy L. Wieder

U.S. Army Engineer Research and Development Center (ERDC)
Cold Regions Research and Engineering Laboratory (CRREL)
72 Lyme Road
Hanover, NH 03755-1290

Eric V. McDonald

Desert Research Institute
Earth and Ecosystem Sciences
2215 Raggio Parkway
Reno, NV 89512

Final Report

Prepared for Assistant Secretary of the Army for Acquisition, Logistics, and Technology
103 Army Pentagon
Washington, DC 20314-1000

Under ERDC 6.2 Geospatial Research and Engineering (GRE) Applied Research Program Army Terrestrial-Environmental Modeling and Intelligence System Science Technology Objective—Research (ARTEMIS STO-R), Work Items T42 P2 448312 and 5L923J, “Geospatial Remote Assessment for Ingress Locations (GRAIL) Project”

Abstract

Connecting landforms to soil strength parameters can enable the prediction of soil bearing capacity and shear strength—important information for mobility and dust emission modeling. This project aimed to relate soil strength metrics to geomorphic landforms, focusing on five alluvial and aeolian landform classes in the Sonoran Desert. To achieve this, a variety of soil strength, dust emission, and soil texture measurements were made at 47 sites in California and Arizona; and these data were compared with landform classifications. Measurements of soil bearing capacity and shear strength varied significantly between landform classes. The aeolian landforms had significantly lower bearing capacity and shear strength than the alluvial landforms. The alluvial fan landform demonstrated consistently high soil strength, whereas the alluvial plain landform had relatively high mean soil strength but extreme site variability. The aeolian landforms were dominated by sand, whereas the alluvial landforms presented variable particle size distributions extending into loam and silt-loam classes. Silt and clay content were positively correlated with soil strength across all sites, while sand content was negatively correlated. Only the near-surface soil strength measures from the pocket penetrometer, Torvane, and vane shear correlated with dust emission flux and susceptibility.

Contents

Abstract ii

Figures and Tables iv

Preface vi

Acronyms and Abbreviations vii

Unit Conversion Factors ix

1 Introduction 1

1.1 Background 1
1.2 Objectives 1
1.3 Approach 2

2 Field testing 3

2.1 Sites 3
2.2 Field tests 8
2.2.1 Clegg 9
2.2.2 Dynamic Cone Penetrometer 10
2.2.3 Cone penetrometer 11
2.2.4 Pocket penetrometer 12
2.2.5 Shear vane measurements 12
2.2.6 Soil volumetric moisture content 13
2.2.7 E-Gauge soil density and moisture content 13
2.2.8 Portable In Situ Wind Erosion Laboratory (PI-SWERL) 14
2.3 Field soil sample analysis 15
2.4 Data analysis 15

3 Results and Discussion 17

3.1 Variations in soil strength with landform type 17
3.2 Cone penetrometer profiles 21
3.3 Soil strength relationships with surface soil composition 24
3.4 Soil strength relationships with dust emission 25

4 Conclusions and Recommendations for Future Work 28

References 30

Appendix A: Supplementary Graphical Data 33

Appendix B: Tabular Soil Strength Data 36

Report Documentation Page

Figures and Tables

Figures

1 SWD and PTD sites in southern California and Arizona. *Clockwise from top left*: Overview map of both study regions, PTD study region, and SWD study region. Basemap by OpenStreetMap 3

2 Examples of the alluvial fan landform (*left*, site SWD40; *right*, site PTD21A) 7

3 Examples of the alluvial plain landform (*left*, site SWD20) and alluvial fan–sand sheet landform (*right*, site SWD24) 7

4 Examples of the dune landform (*left*, site SWD28) and the sand sheet landform (*right*, site SWD46) 7

5 Temperature and precipitation records from weather stations located near the study sites in 2016 9

6 Clegg (*left*) and cone penetrometer (*right*) measurements at site SWD8 10

7 Measuring soil density and moisture using the E-Gauge at site SWD32 13

8 PI-SWERL set up for measurements at site SWD28. The attached carriage is used for transport and holds the battery and software controls 15

9 Comparison of soil strength measurements with landform type. The *p*-values are Kruskal-Wallis one-way analysis of variance 20

10 Mean cone penetrometer profiles for each landform 22

11 Mean cone penetrometer profiles for each landform. Shading is ±1 standard deviation 22

12 Mean DCP CBR soil profiles by landform. Means are calculated on depth values rounded to 25 mm increments 23

13 Mean DCP CBR soil profiles by landform. Means are calculated on depth values rounded to 25 mm increments. Shading represents minimum and maximum limits 23

14 Ternary plot of <2 mm average surface soil texture based on USDA classes 24

15 Spearman correlation matrix of soil strength field measurements, surface soil composition lab measurements, PI-SWERL PM10 flux, and PI-SWERL threshold *u**. The *p*-values are noted as * <0.05, ** <0.01, and *** <0.001 25

16 Linear regression models for dust emission flux with vane shear (*left*), Torvane (*middle*; data available for PTD sites only), and pocket penetrometer (*right*) 26

17 Linear regression models for threshold friction velocity with select surface soil strength metrics. Torvane data are available for only PTD sites 27

A-1 Average cone penetrometer depth profiles for each site 33

A-2 DCP CBR soil profiles for each site 34

A-3 Spearman correlation matrix of soil strength field measurements, PI-SWERL PM10 flux, PI-SWERL threshold *u**, and surface soil composition lab measurements for all sites. The *p*-values are noted as * < 0.05, ** < 0.01, and *** <0.001 35

Tables

1 Site coordinates, landform designations, field descriptions, and U.S. Department of Agriculture (USDA) and Unified Soil Classification System (USCS) soil classes based on soil texture 4

2 General description of the five landforms and associated soil cover 8

3 List of soil strength, composition, and dust emission parameters used in this study 16

4 Summary statistics (mean ± 1 standard deviation) of Clegg, vane shear, and volumetric moisture measurements by landform type 17

5 Summary statistics (mean ± 1 standard deviation) of penetrometer measurements by landform type 17

6 Matrix of strength parameters showing significant difference between landform types based on $p < 0.05$ for both Conover and Iman (1979) and Kruskal-Wallis tests 21

B-1 Averaged soil strength data used in this study. Density is abbreviated as *dens.* and moisture as *moist*. Undisturbed (*undist.*) and disturbed (*dist.*) values are specified for some measurements taken before and after disturbance by hand raking and boot shuffling, respectively 37

B-2 Clegg data for the PTD sites 39

B-3 Average Clegg data for the SWD sites 42

B-4 Cone penetrometer depth profile data. (Depths are in inches.) 43

B-5 Dynamic Cone Penetrometer data for SWD3 to SWD6 46

B-6 Dynamic Cone Penetrometer data for SWD8 to SWD16 48

B-7 Dynamic Cone Penetrometer data for SWD22 to SWD26 50

B-8 Dynamic Cone Penetrometer data for SWD27 to SWD28 52

B-9 Dynamic Cone Penetrometer data for SWD30A to SWD32 53

B-10 Dynamic Cone Penetrometer data for SWD37 to SWD39 55

B-11 Dynamic Cone Penetrometer data for SWD40 to SWD46 56

B-12 Dynamic Cone Penetrometer data for PTD5A to PTD21B 58

B-13 Dynamic Cone Penetrometer data for PTD22 to PTD23E 60

B-14 Dynamic Cone Penetrometer data for PTD25A to PTD26A 62

B-15 Dynamic Cone Penetrometer data for PTD29 to PTD34 64

B-16 Average surface soil USDA texture 66

Preface

This study was conducted for the Assistant Secretary of the Army for Acquisition, Logistics, and Technology as part of the overarching ERDC 6.2 Geospatial Research and Engineering (GRE) Applied Research Program Army Terrestrial Environmental Modeling and Intelligence System Science Technology Objective—Research (ARTEMIS STO-R), Work Items T42 P2 448312 and 5L923J, "Geospatial Remote Assessment for Ingress Locations (GRAIL) Project." The ARTEMIS technical program monitor was Mr. John Eylander, CEERD-RR.

The work was performed by Force Projection and Sustainment Branch (CEERD-RRH) of the Research and Engineering Division (CEERD-RR), U.S. Army Engineer Research and Development Center, Cold Regions Research and Engineering Laboratory (ERDC-CRREL). At the time of publication, Dr. Harley Cudney was Acting Chief, CEERD-RRH, and Mr. J. D. Horne was Chief, CEERD-RR. The Deputy Director of ERDC-CRREL was Mr. David B. Ringelberg, and the Director was Dr. Joseph L. Corriveau.

The authors acknowledge the following people for field support: Mr. Jesse M. Stanley, Jr.; Mr. Bruce Elder; Ms. Samantha Sinclair; Ms. Ariana Sopher; Ms. Karen Foley; Ms. Stacey Jarvis; and Mr. Robert Jones of CRREL and Dr. Mark Sweeney of the University of South Dakota. Ms. Sandra LeGrand and Mr. Matthew Bigl, CRREL, provided manuscript review comments.

COL Ivan P. Beckman was Commander of ERDC, and Dr. David W. Pittman was the Director.

Acronyms and Abbreviations

AF	Alluvial Fan Landform
AP	Alluvial Plain Landform
ARTEMIS	Army Terrestrial Environmental Modeling and Intelligence System
ASABE	American Society of Agricultural and Biological Engineers
ASAE	American Society of Agricultural Engineers
Av	Vesicular A
$CaCO_3$	Calcium Carbonate
CBR	California Bearing Ratio
CH	Inorganic Silts
CI	Cone Index
CIV	Clegg Impact Value
CL	Clays
CRREL	Cold Regions Research and Engineering Laboratory
D	Dune Landform
DCP	Dynamic Cone Penetrometer
DRI	Desert Research Institute
ERDC	U.S. Army Engineer Research and Development Center
GRAIL	Geospatial Remote Assessment for Ingress Locations
GRE	Geospatial Research and Engineering
LOI375	Loss-on-Ignition at 375° for 4 hours
PI-SWERL	Portable In Situ Wind Erosion Laboratory
PM10	Particulate Matter Less than μm in Diameter

PTD	Phoenix-Tucson Dust
RPM	Revolutions per Minute
SS	Sand Sheet Landform
STO-R	Science Technology Objective—Research
SWD	Southwest Dust
USCS	United Soil Classification System
USDA	U.S. Department of Agriculture
Y	Young

Unit Conversion Factors

Multiply	By	To Obtain
cubic feet	0.02831685	cubic meters
degrees (angle)	0.01745329	radians
degrees Fahrenheit	(F-32)/1.8	degrees Celsius
feet	0.3048	meters
inches	0.0254	meters
microinches	0.0254	micrometers
mils	0.0254	millimeters
pounds (force)	4.448222	newtons
pounds (force) per square inch	6.894757	kilopascals
pounds (mass)	0.45359237	kilograms
pounds (mass) per cubic foot	16.01846	kilograms per cubic meter
square inches	6.4516 E-04	square meters
square yards	0.8361274	square meters
yards	0.9144	meters

1 Introduction

1.1 Background

Physical characterization of the operational environment is needed to address issues facing the military, such as logistics and maneuverability, air and ground vehicle mobility, windblown and fugitive dust degradations to visual and sensing environments, and impacts to cover and concealment. However, limited spatial and temporal empirical data constrain ongoing efforts to model and predict terrain features. As empirical data for specific regions of interest can be difficult to obtain, there has been a recent focus in the research community on connecting terrain characteristics with remotely assessed geomorphology.

Geomorphology and landscape processes form the basis of soil characteristics. A skilled geomorphologist can evaluate the landform processes of regional areas using remotely sensed, satellite-based images to classify terrain based on geomorphic landform type. However, the empirical relationships between geomorphology and soil parameters of interest, such as soil strength and dust emission, remain poorly defined for many regions.

Linking landform geomorphology and soil characteristics is a continuing line of research. McDonald et al. (2013) worked over a 9-year span to develop an integrated, predictive tool for forecasting desert terrain conditions with regard to several variables, including soils, dust emission potential, and trafficability or mobility hazards, to support military activities in desert environments. They developed multiple approaches using basic terrain data, including remotely sensed data and imagery, to predict detailed surfaces and subsurface terrain conditions over a wide range of scales in near real time. Other recent efforts have also used remotely sensed data to create geomorphic maps that predict dust emission potential at scales ranging from individual deserts to continents (Parajuli and Zender 2017; Bullard et al. 2011) and using remotely sensed data to infer soil strength (Sopher et al. 2016a, 2016b).

1.2 Objectives

The primary objective of this study was to determine whether significant relationships exist between soil strength parameters (i.e., bearing capacity

and shear strength) and geomorphic landform type in the Sonoran Desert region. Secondarily, the study explored soil strength relationships with soil composition (i.e., particle size, moisture, and organic and carbonate contents) and with dust emission potential. These empirical relationships assist in efforts to remotely assess soil characteristics.

1.3 Approach

To accomplish these objectives, the U.S. Army Engineer Research and Development Center's Cold Regions Research and Engineering Laboratory (ERDC-CRREL) partnered with the Desert Research Institute (DRI), the nonprofit environmental research arm of the Nevada System of Higher Education, to collect data on soil strength, soil properties, and dust emission potential across a range of geomorphic landforms in the Sonoran Desert.

2 Field testing

2.1 Sites

ERDC-CRREL and DRI researchers conducted two field campaigns in 2016. The Southwest Dust (SWD) field campaign was conducted from 18 to 23 May and focused on southern California and southwestern Arizona in the Colorado Desert subregion of the Sonoran Desert. SWD sites are generally along Interstate 8 in the vicinity of El Centro, California, and Yuma, Arizona. The Phoenix-Tucson Dust (PTD) field campaign was conducted from 16 to 20 September and focused on sites in southern Arizona in the Sonoran Desert. PTD sites are along Interstate 10 in the vicinity of Casa Grande and Eloy, Arizona (Figure 1). Table 1 lists the locations, site descriptions, and soil texture classifications for each site. Data from each site was labeled with the field campaign, a number, and in some cases a letter if more than one area was tested at a site (i.e., PTD21A).

Figure 1. SWD and PTD sites in southern California and Arizona. *Clockwise from top left*: Overview map of both study regions, PTD study region, and SWD study region. Basemap by OpenStreetMap.

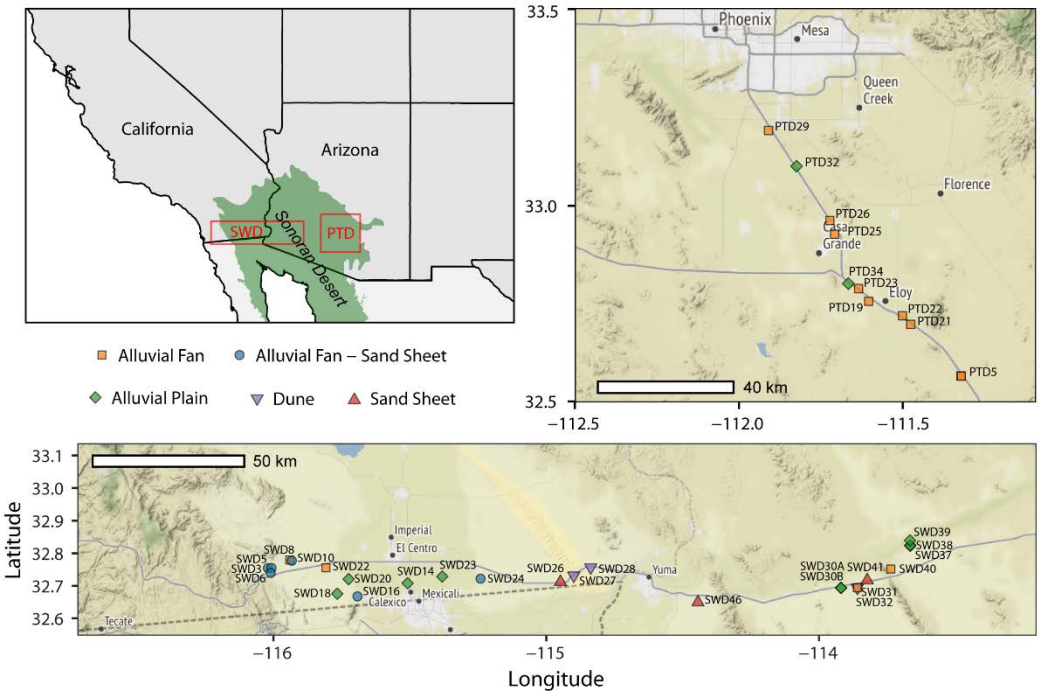

Table 1. Site coordinates, landform designations, field descriptions, and U.S. Department of Agriculture (USDA) and Unified Soil Classification System (USCS) soil classes based on soil texture.

Site	Date	Latitude	Longitude	Landform	Description	USCS Class	USDA Class
SWD3	5/18/2016	32.755	−116.020	Alluvial Fan–Sand Sheet	Loose sandy soil, coppice dunes, within ~1 km of wind turbines	SP-SM	Fine Sand
SWD5	5/18/2016	32.755	−116.007	Alluvial Fan–Sand Sheet	Decomposed granite of sand and gravel size, sandy soil, typical soil cover	SM	Fine Sand
SWD6	5/18/2016	32.740	−116.010	Alluvial Fan–Sand Sheet	Loose sandy soil, coppice dunes, active ripples	SP-SM	Fine Sand
SWD8	5/19/2016	32.779	−115.940	Alluvial Fan	Gravel-pebble weak pavement, disturbed site (tracks), sand/dust emitter when disturbed	SM	Sandy Loam
SWD10	5/19/2016	32.777	−115.933	Alluvial Fan–Sand Sheet	Loose sandy soil, coppice dunes, marginal active channel	SW/SP	Fine Sand
SWD14	5/19/2016	32.708	−115.508	Alluvial Plain	Fallow field, El Centro basin, Lake Cahuilla sediments, mudcracks with ~0.5 cm crust	ML-CL	Silt Loam
SWD16	5/19/2016	32.668	−115.692	Alluvial Fan–Sand Sheet	Decomposed granite of sand size, coppice dunes, ripples	SW/SP	Fine Sand
SWD18	5/19/2016	32.676	−115.766	Alluvial Plain	Active ephemeral wash, loose sand, ripples	SM	Silt Loam
SWD20	5/20/2016	32.721	−115.725	Alluvial Plain	Lake Cahuilla sandy silt sediments, polygonal silt crust	SP-SM	Sandy Loam
SWD22	5/18/2016	32.756	−115.808	Alluvial Fan	Pavement, disturbed (tracks)	SM-SC/SC	Silt Loam
SWD23	5/20/2016	32.729	−115.381	Alluvial Plain	Fallow field, very hard surface	SM	Sandy Loam
SWD24	5/20/2016	32.722	−115.241	Alluvial Fan–Sand Sheet	Coppice dunes, silty crust in interspace, Colorado river sediment	SM	Loamy Fine Sand
SWD26	5/20/2016	32.712	−114.948	Sand Sheet	Just west of Algodones Dunes, large coppice dunes, sandy interspace, ripples	SW/SP	Fine Sand
SWD27	5/20/2016	32.732	−114.899	Dune	Interior of Algodones Dunes, in Off-Highway Vehicle area, moisture at ~2 cm depth	SW/SP	Fine Sand
SWD28	5/21/2016	32.757	−114.837	Dune	Just east of Algodones Dunes, small (2–4 m) dunes, sandy interspace, ripples, active	SW/SP	Fine Sand
SWD30A	5/22/2016	32.694	−113.920	Alluvial Plain	Small coppice dunes, sandy interspace, crust/hardpan revealed by PI-SWERL ~4 cm depth	SM	Loamy Fine Sand
SWD30B	5/22/2016	32.694	−113.920	Alluvial Plain	Disturbed plowed surface, no vegetation	SM	Fine Sand

Table 1 (cont.). Site coordinates, landform designations, field descriptions, and USDA and USCS soil classes based on soil texture.

Site	Date	Latitude	Longitude	Landform	Description	USCS Class	USDA Class
SWD31	5/22/2016	32.694	−113.860	Dune	North–south liner dunes, loose sandy soil, dune top with ripples, ambrosia, moisture at ~6–8 cm depth	SW/SP	Fine Sand
SWD32	5/22/2016	32.694	−113.860	Alluvial Fan	Pebble-lag/silty crust soil, between liner dunes, high sand/dust emitter, black ~2–5 cm bionodules, <1 cm biocrust	ML	Sandy Loam
SWD37	5/22/2016	32.823	−113.666	Alluvial Plain	Gila River broad active channel, disturbed (bladed) with mixed sediments, no ripples	SW/SP	Fine Sand
SWD38	5/22/2016	32.824	−113.666	Alluvial Plain	Gila River floodplain, silty-sandy sediments, *tamarix* sp.	SM	Sandy Loam
SWD39	5/22/2016	32.839	−113.667	Alluvial Plain	Gila River alluvial plain, silty-sandy sediments, mesquite, mostly undisturbed	ML-CL	Silt Loam
SWD40	5/23/2016	32.748	−113.737	Alluvial Fan	Late Holocene distal fan, weak gravel pavement, biocrust in places	SM	Sandy Loam
SWD41	5/23/2016	32.717	−113.824	Sand Sheet	Sandy soil, coppice dunes, critter holes, dust/sand emitter under moderate winds	SP-SM/SM	Fine Sand
SWD46	5/21/2016	32.649	−114.444	Sand Sheet	Dune/loose sandy soil, scattered grass shrubs, ripples	SW/SP	Fine Sand
PTD5A	9/20/2016	32.566	−111.323	Alluvial Fan	Playa, curled mudcracks	ML	Silt
PTD5B	9/20/2016	32.565	−111.322	Alluvial Fan	Non-mudcracked surface, sand covered, ~100 m from PTD5A	ML	Silt Loam
PTD8A	9/20/2016	32.512	−111.293	Not classified	Former agricultural area, untracked site, sparse shrubs/bushes, patches of grass	ML	Silt Loam
PTD8B	9/20/2016	32.512	−111.293	Not classified	Tracked site ~30 m from PTD8A, fresh tire tracks	CL	Sandy Loam
PTD19	9/19/2016	32.756	−111.604	Alluvial Fan	Plowed/disced ~2005, Glenbar clay loam, polygonal ~1 cm crust	ML-CL	Silt Loam
PTD21A	9/19/2016	32.700	−111.480	Alluvial Fan	Limited disturbance, stands of *larrea* sp., small sand ripples, marginal areas sandy, likely high dust emitter	SM	Sandy Loam
PTD21B	9/19/2016	32.698	−111.476	Alluvial Fan	Unvegetated, mudcracks with pebble and gravel sized clasts	CL	Silt Loam
PTD22	9/19/2016	32.719	−111.501	Alluvial Fan	Sparse vegetation, vehicle tracks, not plowed, red clay loam, mudcrack crust with sand cover, sand ripples	ML-CL	Silt Loam
PTD23A	9/18/2016	32.789	−111.635	Alluvial Fan	Well-developed black soil crust, small coppice dunes	ML-CL	Silt Loam

Table 1 (cont.). Site coordinates, landform designations, field descriptions, and USDA and USCS soil classes based on soil texture.

Site	Date	Latitude	Longitude	Landform	Description	USCS Class	USDA Class
PTD23B	9/18/2016	32.789	−111.634	Alluvial Fan	Deflating large coppice dunes, mesquite, animal burrows, likely high dust emitter	ML	Loam
PTD23C	9/18/2016	32.788	−111.633	Alluvial Fan	Deflating surface, mesquite roots at surface, degraded plant mounds, wide mudcracks not curled/lifted	CL	Silt Loam
PTD23D	9/18/2016	32.789	−11.634	Alluvial Fan	Curled mudcracks, interspersed bushes	ML-CL	Silt Loam
PTD23E	9/18/2016	32.779	−111.612	Alluvial Fan	Plowed or tilled before 1996, never farmed, furrows weak but visible, surface thin silt-sand polygonal crust with curled edges, small annuals trapping silty-sand	ML	Silt Loam
PTD25A	9/16/2016	32.928	−111.708	Alluvial Fan	Plowed or tilled before 1996, never farmed, furrows weak, but visible, surface lag cover, discontinuous <2 mm streaks of silty crust, patches of small annuals trapping silty-sand	SM	Sandy Loam
PTD25B	9/16/2016	32.932	−111.705	Alluvial Fan	Sandy soil cover, coppice mounds, numerous deflated areas visible	SM	Sandy Loam
PTD25C	9/16/2016	32.928	−111.708	Alluvial Fan	Plowed or tilled before 1996, never farmed, furrows weak, but visible, surface lag cover, discontinuous <2 mm streaks of silty crust, patches of small annuals trapping silty-sand	ML	Sandy Loam
PTD26A	9/17/2016	32.966	−111.726	Alluvial Fan	Unplowed area ~100 m from PTD26B, small coppice mounds, patches of black biocrust, weak lag cover	ML	Sandy Loam
PTD26B	9/17/2016	32.963	−111.722	Alluvial Fan	Plowed or tilled before 1997, no farming after ~2005, furrows mostly intact and visible, surface thin-moderate (3–6 mm) silt-sand crust, breaks when walked upon	ML	Sandy Loam
PTD29	9/17/2016	33.192	−111.909	Alluvial Fan	Complex area of large coppice dunes and silt/clay interspace areas, possible high dust emitter	SM	Sandy Loam
PTD32A	9/17/2016	33.100	−111.823	Alluvial Plain	Natural/undisturbed analog to PTD32B, ~100 m from PTD32B	ML	Silt Loam
PTD32B	9/17/2016	33.101	−111.824	Alluvial Plain	Plowed field of very loose silt with ~1 cm mudcrack crust	ML	Silt Loam
PTD34	9/19/2016	32.802	−111.666	Alluvial Plain	Solid flat sand and pebble-covered surface, larger bushes nearby and sparse grass	ML	Silt Loam

DRI selected the field sites to cover a diverse range of desert geomorphology. An experienced desert geomorphologist and soil scientist (Eric McDonald, DRI) categorized each site into five geomorphic landforms: alluvial fan (AF), alluvial plain (AP), alluvial fan–sand sheet (AF-SS), sand sheet (SS), and dune (D). The landform classifications used were developed as part of a companion project to look at dust emission across portions of southern Arizona, California, and northern Mexico (McDonald et al. 2018; Bacon and McDonald 2016). Figures 2 through 4 show examples of the landforms, and Table 2 gives a geomorphological description of each landform.

Figure 2. Examples of the alluvial fan landform (*left*, site SWD40; *right*, site PTD21A).

Figure 3. Examples of the alluvial plain landform (*left*, site SWD20) and alluvial fan–sand sheet landform (*right*, site SWD24).

Figure 4. Examples of the dune landform (*left*, site SWD28) and the sand sheet landform (*right*, site SWD46).

Table 2. General description of the five landforms and associated soil cover.

Landform	General Description	General Soil Condition
Dune (D)	Small to large hills (tens of meters in height) of various morphologies. Surface layer of sand loose due to frequent mobilization under moderate to strong winds.	No soil development; loose sand with depositional bedding common.
Sand Sheets (SS)	Alluvial fans or plains covered in fine sediments composed of loose and well-sorted sand. Pockets or areas of vegetation common. Small mounds or dunes (~<10 m) to coppice dunes around vegetation common.	Primarily no soil development, but locally very weekly developed soils possible where sand has been stabilized by vegetation.
Alluvial Fans with Sand Sheets (AF-SS)	Commonly distal fans with discontinuous sand dunes, sheets, or coppice mounds. Sand cover commonly thin (< 1m) and of low density with lateral coverage generally of <5% cover. Deposited sand commonly covers older alluvium.	Variable soil development. No soil developed in active windblown sand, and weakly to strongly developed soils developed in underlying alluvium. The soil surface where not covered by sand commonly has either a weak discontinuous pebble-gravel lag or weakly to moderately developed desert pavement.
Alluvial Fans-Young (AF-Y)	Alluvium associated with desert ephemeral channels draining mountain basins. Commonly composed of sand-rich sediments with a low to high abundance of gravel and cobbles. Young alluvial fans were deposited within the last ~10,000 years (Holocene).	Variable soil development ranging from weakly to moderately developed. Vesicular A (Av) horizons common. Fan surfaces have either no desert pavement to moderately developed desert pavement.
Alluvial Plains-Young (AP-Y)	Alluvium terraces and valley fill deposits associated with ephemeral to perennial channels. Commonly composed of silt- to sand-rich sediments with a low to high abundance of gravel and cobbles. Young alluvial plains were deposited within the last ~10,000 years (Holocene).	Desert pavements not common; or if present, weakly developed. Soils vary from weakly to moderately developed. Soils and deposits can be highly variable in texture.

2.2 Field tests

Field testing occurred during the two campaigns in May (SWD sites) and September (PTD sites) of 2016 (Figure 1). All tests for each site occurred on the same day over a 2 to 4 hour period within a roughly 200 m^2 (240 yd^2) area that was flagged at each corner. Influence by the sparse desert vegetation was avoided by testing on unvegetated and undisturbed surfaces. Conditions were dry and sunny during the SWD section and were a mix of humid/overcast and dry/sunny during the PTD section. About

0.5 cm (0.2 in.) of precipitation was recorded at weather stations near the study sites on the day before the SWD field campaign began and about a week before the PTD field campaign (Figure 5).

Figure 5. Temperature and precipitation records from weather stations located near the study sites in 2016.

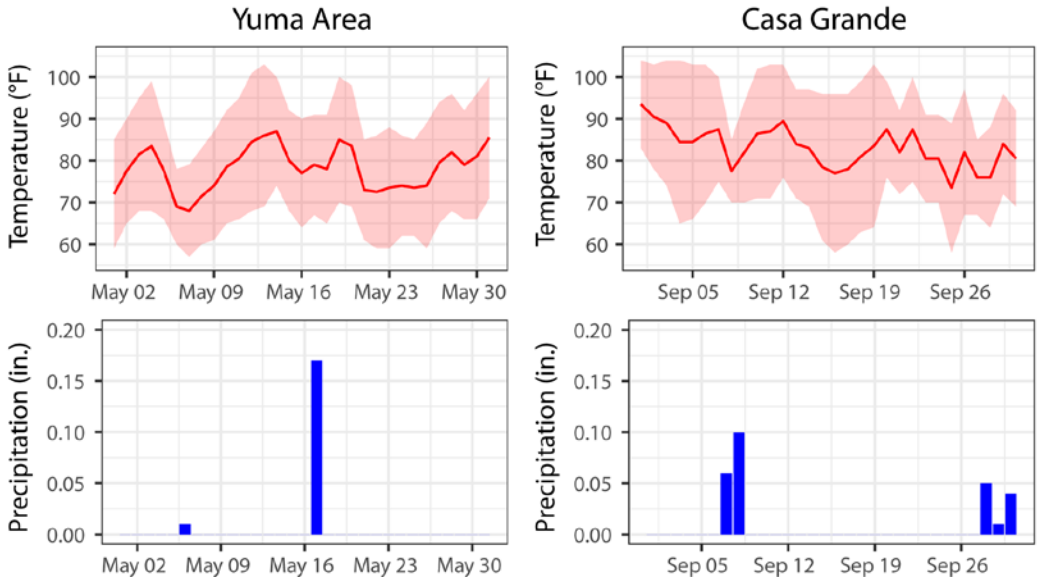

Field tests specifically testing for soil strength included measures of bearing capacity (i.e., Clegg Impact Hammer [Clegg] and penetrometers) and shear strength (i.e., shear vanes). Two large penetrometers were used: a Field Scout SC900 cone penetrometer (henceforth the cone penetrometer), which offers rapid measurement, and the Dynamic Cone Penetrometer (DCP), which is better suited for hard soils and takes measurements deeper (up to 1 m [39 in.]) into the subsurface. A pocket penetrometer was used to measure the bearing capacity of the soil surface. In the case of both the DCP and the Clegg, empirically derived relationships enable the calculation of California Bearing Ratio (CBR), the current bearing capacity standard for the Army. Soil properties, which relate to soil strength, were also measured in the field, including moisture content and density.

2.2.1 Clegg

The Clegg consists of a cylindrical mass hammer that is dropped within a guide tube from a set height (Clegg 1980; ASTM 2016). The hammer is equipped with an accelerometer that measures the peak deceleration on impact in gravity units. The hammer is dropped several times at each location, and deceleration readings are recorded for each drop. The readings

are reported in 1/10 g-forces. Typically, both the 2.25 kg (5.0 lb) and the 0.5 kg (1.1 lb) size Cleggs are used to measure natural ground surfaces. Shoop et al. (2012) provides a good summary and background on the different Clegg sizes, their uses, and conversion to other soil strength parameters.

Clegg measurements were taken at each site using both the 2.25 kg hammer and the 0.5 kg hammer at each corner of a flagged rectangular area approximately 10 × 10 m (33 × 33 ft) (Figure 6).

Figure 6. Clegg (*left*) and cone penetrometer (*right*) measurements at site SWD8.

Clegg Impact Values (CIVs) for each site were taken as the average measurement of the third drop, for the 2.25 kg Clegg, and the fourth drop, for the 0.5 kg Clegg, at each corner. CIV values were converted to CBR following equation (1) for the 2.25 kg Clegg data and equation (2) for the 0.5 kg Clegg data (Shoop et al. 2012; Millar 1977).

$$CBR\ (\%) = e^{\frac{10\ CIV_{2.25kg} - 14.936}{79.523}}. \quad (1)$$

$$CBR\ (\%) = 0.55\ CIV_{0.5kg} - 1. \quad (2)$$

2.2.2 Dynamic Cone Penetrometer

ASTM (2015) D6951/D6951M-09 gives the DCP test apparatus and procedures. The DCP is used heavily by the U.S. Air Force to evaluate bearing capacity and soil strength profiles for both paved and unsurfaced airfields. Either the 4.6 kg (10.1 lb) or the 8 kg (17.6 lb) sliding drop hammer was

used, depending on the strength of the soils at a particular site, along with the standard 60 degree, 20 mm (0.787 in.) diameter cone tip. The soil strength was determined by measuring the penetration of the cone into the soil after each hammer drop or series of hammer drops for stronger soil.

In this study, the DCP measurements were taken to a depth of approximately 1 m (39 in.) or until refusal after 40 consecutive blows. The DCP index is the depth in millimeters per blow and was averaged into 0–150 mm (0–6 in.) depth, 150–300 mm (6–12 in.) depth, and full depth (i.e., 0–39 in.). A hammer factor of 1 was applied for the DCP index when using the heavy 8 kg hammer and a factor of 2 when using the light 4.6 kg hammer. In addition, the initial depth of penetration of the DCP with only the static weight was also recorded. DCP index values were converted to CBR following ASTM (2015), which prescribes equations depending on the soil's Unified Soil Classification System (USCS) soil type. Equation (3) was used for all soils except inorganic silts (CH) or clays (CL) with CBR less than 10, and equation (4) was used for CL soils with CBR below 10:

$$CBR\ (\%) = \frac{292}{DCPindex^{1.12}}. \quad (3)$$

$$CBR\ (\%) = \frac{1}{(0.017019\ DCPindex)^2}. \quad (4)$$

Equation (3) was applied to DCP indices in depth profiles for each site, except for three sites (PTD21B, PTD23C, and PTD8B) that had the USCS class "CL" where equation (4) was applied as they met the criterion for CBR values less than 10 (ASTM 2015). USCS soil classes were estimated by comparing the soil texture with the U.S. Department of Agriculture (USDA) ternary diagram (García-Gaines and Frankenstein 2015). USCS soil classes were used in this study only to apply the correct CBR calculation. Table 1 shows the correlation between the two soil classification systems for these test sites.

2.2.3 Cone penetrometer

The cone penetrometer, also known as the Trafficability Cone Penetrometer, is used extensively by the U.S. Army. It is a simple instrument designed to give a Cone Index (CI) of soil strength quickly and easily. U.S. Army Field Manual 5-430-00-1 (U.S. Army 1994) and American Society of

Agricultural Engineers (ASAE)* Standard S313.3 (ASABE 2006a) provide instructions for its use. The cone penetrometer used in this study was the Field Scout SC 900 Soil Compaction Meter (Spectrum Technologies 2013) with the 12.7 mm (0.5 in.) diameter cone (base area 516 mm^2 [0.8 $in.^2$]). The Field Scout reported CI in kilopascals (kPa), which is the agricultural community standard (ASABE 2006b). The cone was pressed into the soil at a uniform rate of approximately 30 mm/s (72 in./min) although this rate may not have been achieved in harder soils. The first reading was taken when the base of the cone was flush with the soil surface and then every 25 mm (1 in.) thereafter. The cone penetrometer value for each site is the average of three to eight measurements.

2.2.4 Pocket penetrometer

The Geotester dial penetrometer (henceforth pocket penetrometer) estimates the unconfined compressive strength of the soil surface in kilograms per square centimeter when used with the standard 6.35 mm (0.25 in.) diameter plunger. Four larger plungers of 10, 15, 20, and 25 mm (0.39, 0.59, 0.79, and 0.98 in.) diameters can provide strengths over a wide range of cohesive soil types.

The plunger of the pocket penetrometer was pressed into the soil until the soil collapsed or to the calibration notch. The penetrometer was withdrawn from the soil with the test value retained on the dial. Dial readings were manually recorded and later converted to soil bearing capacity by using calibration charts provided by the manufacturer (AMS 2018). As soil strength varied considerably between sites, different plunger sizes were used. Three measurements or more were taken at each site and were averaged.

2.2.5 Shear vane measurements

Measurements of surface shear strength were made using a Pilcon Hand Shear Vane Tester (henceforth vane shear) and, at the PTD sites only, a Durham Geo Torvane. Both techniques are simple in that the vanes are inserted into the soil to a depth at least covering the entire vane, and then a steady turning force is applied until the soil shears. The maximum shear force is recorded on the instrument dial as kilopascals for the vane shear and kilograms per square meter for the Torvane. The vane shear is a standard piece of soil testing equipment, but there are no U.S. standards

* The name of the organization has since been changed to the American Society of Agricultural and Biological Engineers (ASABE).

for use. Several vane sizes are available for the vane shear, but this study consistently used the 19 mm (0.75 in.) diameter and the 33 mm (1.3 in.) diameter vanes. The shear strength values for each site are the average of three measurements.

2.2.6 Soil volumetric moisture content

A Field Scout TDR 300 (Spectrum Technologies, Inc.) moisture meter was used at each corner of the field site. The meter calculates volumetric water content by measuring conductivity between two rods. The manufacturer reports an accuracy of ±3.0% in soils with conductivity less than 2000 µS/cm, a condition met at all sites (which ranged from 3 to 294 µS/cm). The 76 mm (3 in.) long rods were pushed fully into the soil. Volumetric moisture values for each site are the average of four measurements.

2.2.7 E-Gauge soil density and moisture content

The Troxler E-Gauge uses a low-level Cesium-137 source to measure wet soil density by gamma radiation backscatter with high accuracy (Berney et al. 2016). Measurements were made at 5 cm (2 in.) and 10 cm (4 in.) soil depths in an approximately 2 cm (0.8 in.) diameter preformed hole. The E-Gauge also measures gravimetric soil moisture using a separate probe (Figure 7).

Figure 7. Measuring soil density and moisture using the E-Gauge at site SWD32.

2.2.8 Portable In Situ Wind Erosion Laboratory (PI-SWERL)

As shown in Figure 8, dust emission was measured using a PI-SWERL (30 cm [11.8 in.] diameter) connected to a DustTrak II Aerosol Monitor 8530 with an inlet selective of particulate matter less than 10 μm (0.4 mils) in diameter (PM10) (Etyemezian et al. 2007, 2014). PI-SWERL measurements at each site typically began with a ramp test followed by a set (3–5 replicates) of step tests at undisturbed areas within approximately 1–2 m (3–6 ft) of each other. The ramp test linearly increases the revolutions per minute (RPM) of the PI-SWERL's annular blade from 0 to 4000–6000, with the end RPM selected based on the expected emissivity of the soil, over 5 minutes. The step test follows a program of three steps of increasing RPM, starting with a cleaning stage of 0 RPM from 0 to 60 seconds, a linear increase in RPM to the first step over 45 seconds, a hold at the first step RPM for 90 seconds, and then a repetition of this linear increase and hold for two more sequential steps. The full step test takes approximately 5 minutes. The target RPM of each step varied for each site and was based on the emissivity of the soil to avoid saturating the DustTrak (PM10 > 200 mg m^{-3}). Steps were set to 1000, 2000, and 3000 RPM for high emissivity soils; 2000, 3000, 4000 RPM for medium-high emissivity soils; 3000, 4000, 5000 RPM for medium-low emissivity soils; and 4000, 5000, 6000 RPM for low emissivity soils. PM10 dust flux was calculated at each RPM level of the step tests in units of milligrams per square meter per second (mg m^{-2} s^{-1}). An estimated effective wind friction velocity (u^*) was calculated for each RPM level following the method of Etyemezian et al. (2014) by using the lookup-table surface roughness correction. To compare sites at the same u^*, PM10 fluxes were estimated at an effective u^* of 0.7 m s^{-1} (2.3 ft/s) using the near-linear relationship between u^* and the logarithm of PM10 flux. Threshold RPM values for saltation-driven dust emission are estimated as the inflection point of PM10 concentrations during the linear ramp-up test and ramp portions of the step test, with supporting evidence from saltation optical gate sensor data. Threshold RPM values were converted to effective threshold values u^* (u^*_t) using the roughness correction (Etyemezian et al. 2007, 2014).

Figure 8. PI-SWERL set up for measurements at site SWD28. The attached carriage is used for transport and holds the battery and software controls.

2.3 Field soil sample analysis

CRREL collected triplicate surface (0–1 cm [0–0.4 in.] depth) soil samples at each site. These samples were subsampled for gravimetric water content by loss-on-drying at 110°C (230°F) for 8 hours, organic content by loss-on-ignition at 375°C (707°F) for 4 hours (LOI375), and calcium carbonate ($CaCO_3$) content by 4 M acetic acid extraction with calcium analysis by Inductively Coupled Plasma Optical Emission Spectroscopy. Particle size analysis was also measured with a Horiba LA-960A on 1 g soil samples disaggregated in 30 mL solutions of sodium hexametaphosphate (38 g/L). Particle sizes were binned by USDA definitions into clay (<0.002 mm), silt (0.002–0.05 mm), and sand (0.05–2.00 mm).

2.4 Data analysis

Correlations, analysis of variance, and statistical tests were performed in R 3.4 (R Core Team 2017). Nonparametric statistical methods were employed due to the nonnormality of data typical of some measurement techniques. These include Spearman rank correlation, Kruskal-Wallis one-way analysis of variance, and the Conover-Iman test (Conover and Iman 1979). Linear regression models were built for some log-transformed measurements. Table 3 lists all measurements and their units.

Table 3. List of soil strength, composition, and dust emission parameters used in this study.

Parameter	Units	Description
CBR 2.25 kg	%	California Bearing Ratio from 2.25 kg Clegg
CBR 0.5 kg	%	California Bearing Ratio from 0.5 kg Clegg
Clegg 2.25 kg	CIV	Clegg Impact Value from 2.25 kg Clegg
Clegg 0.5 kg	CIV	Clegg Impact Value from 0.5 kg Clegg
Cone Pen. 1–6 in.	kPa	Average cone penetrometer reading from 1–6 in. depth
DCP initial	mm	DCP initial depth
DCP 0–6 in.	-	DCP index 0–6 in. depth averaged
DCP 6–12 in.	-	DCP index 6–12 in. depth averaged
DCP Full	-	DCP index full depth averaged
Pocket Pen.	kg cm^{-2}	Pressure from pocket penetrometer
Vane Shear	kPa	Pilcon vane shear at surface
Torvane	kg cm^{-2}	Torvane at surface
Volumetric Moisture	%	Field Scout volumetric moisture content at 3 in. depth
E-Gauge Dry Density 2 in.	lb ft^{-3}	Dry density at 2 in. depth
E-Gauge Dry Density 4 in.	lb ft^{-3}	Dry density at 4 in. depth
E-Gauge Moisture 2 in.	%	Gravimetric moisture content at 2 in. depth
E-Gauge Moisture 4 in.	%	Gravimetric moisture content at 4 in. depth
Gravimetric Moisture	wt %	Lab gravimetric moisture content from drying at 105°C
LOI375	wt %	Loss-on-Ignition at 375 °C—proxy for organic content
Clay	vol %	USDA clay in <2 mm soil fraction
Silt	vol %	USDA silt in <2 mm soil fraction
Sand	vol %	USDA sand in <2 mm soil fraction
$CaCO_3$	%	Calcium carbonate
PM10 Flux	mg m^{-2} s^{-1}	PI-SWERL estimated PM10 flux at an effective u^* of 0.7 m s^{-1}
u^*_t	m s^{-1}	PI-SWERL estimated effective threshold friction velocity (u^*) for saltation-driven PM10 emission

3 Results and Discussion

3.1 Variations in soil strength with landform type

Tables 4 and 5 summarize the results of each soil strength test by landform type. CBR values derived from the two Cleggs were generally less than 10, typical of sands, silts, and clays (Yoder and Witczak 1975). Volumetric moisture contents of 2%–5% are consistent with arid lands. The DCP indices, which are inversely related to soil bearing capacity, showed increasing bearing capacity with depth for each of the landforms. This is typical for undisturbed, homogeneous soils. The DCP initial depth metric (the depth that the DCP penetrated into the surface prior to dropping the weight package) varied between 4 and 12 cm (1.6 and 4.7 in., respectively), indicating very loose, unconsolidated surface soils at some sites. Comparing strength between landform types, the alluvial landforms tended to have greater bearing capacity (i.e., Cleggs and penetrometers) and shear strength compared with the aeolian dune and sand sheet landforms.

Table 4. Summary statistics (mean ± 1 standard deviation) of Clegg, vane shear, and volumetric moisture measurements by landform type.

Landform	*n*	CBR 0.5 kg	CBR 2.25 kg	CIV 0.5 kg	CIV 2.25 kg	Vane Shear (kPa)	Volumetric Moisture (%)
AF	21	9.2 ± 3.2	3.8 ± 2.0	18.7 ± 5.9	19.9 ± 4.1	15.8 ± 8.4	5.3 ± 2.1
AF-SS	6	6.4 ± 1.4	2.5 ± 1.1	13.5 ± 2.6	8.3 ± 3.5	5.9 ± 4.3	2.18 ± 0.46
AP	12	8.3 ± 6.4	2.6 ± 1.7	17 ± 12	8.0 ± 5.0	8.5 ± 7.4	5.2 ± 5.9
D	3	5.2 ± 0.6	1.3 ± 0.3	11.3 ± 1.1	3.4 ± 1.9	2.1 ± 0.1	3.2 ± 1.1
SS	3	5.6 ± 1.6	1.5 ± 0.3	11.9 ± 3.0	4.8 ± 1.7	2.5 ± 1.1	2.6 ± 1.1

Table 5. Summary statistics (mean ± 1 standard deviation) of penetrometer measurements by landform type.

Landform	Pocket Pen (kg cm^{-2})	Cone Pen 1–6 in. (kPa)	DCP 0–6 in. Index	DCP 6–12 in. Index	DCP Full Index	DCP Initial (mm)
AF	5.5 ± 7.6	2530 ± 820	39 ± 19	24 ± 16	18 ± 13	68 ± 47
AF-SS	5.0 ± 3.9	1630± 450	79 ± 55	58 ± 24	19.9 ± 5.4	122 ± 80
AP	7.9 ± 6.8	1600 ± 1000	62 ± 38	59 ± 70	27 ± 35	123 ± 91
D	0.77 ± 0.21	600 ± 250	188 ± 30	129 ± 73	130 ± 110	49 ± 17
SS	2.2 ± 2.0	1150 ± 290	112 ± 28	49.5 ± 2.4	29.7 ± 5.3	35.8 ± 1.4

Figure 9 and Table 6 show the results of statistical tests of soil strength differences between landforms. Kruskal-Wallis analysis of variance was performed alongside boxplots shown in Figure 9. Soil strength metrics exhibiting a significant difference in Kruskal-Wallis tests were then subjected to Conover-Iman tests to examine differences between individual landforms (Table 6).

CIV and calculated CBR values from both the 2.25 kg and 0.5 kg Clegg were significantly different between the five landforms (Kruskal-Wallis p-value < 0.05; Figure 9). Based on this CIV (and CBR) data, alluvial fan sites had consistently high values, dune and sand sheet sites had consistently low values, alluvial fan–sand sheet sites had intermediate values, and alluvial plain sites had highly variable values. Subsequent Conover-Iman tests indicated that only the alluvial fan landform was statistically different from each of the other landforms in terms of CIVs (Table 6).

Although the alluvial fan landform overall exhibited high soil surface hardness, an exceptionally weak site that was formerly a plowed or tilled field (PTD26B) was also represented by this landform. Similarly within the alluvial plain landform, another formerly plowed or tilled field (PTD32B) had the lowest CIVs across all sites. One site located within the Gila River channel (SWD37) and another one nearby (SWD38) also had exceptionally low strength.

Surface soil shear strength was significantly higher for the alluvial fan landform than for all other landforms (Table 6 and Figure 9). Again, the previously plowed alluvial fan site mentioned above (PTD26B) also had outlying low shear strength (Figure 9). Although the dune and sand sheet landforms had consistently low shear strength, they were not significantly different from the other alluvial landforms.

Volumetric moisture of the top 76 mm (3 in.) of the alluvial fan landform was significantly greater than that for the alluvial fan–sand sheet, alluvial plain, and sand sheet landforms, but not significantly different from the dune landform. The alluvial plain landform had significantly greater moisture at the surface than the alluvial fan–sand sheet landform, but it was not significantly different from the other landforms.

The pocket penetrometer measurements did not yield significant differences between landform types (Table 6 and Figure 9). The failure to reject

the null hypothesis (i.e., that at least one of the landforms is different) was likely driven by the low within-landform sample size. As expected, dune and sand sheet landforms had generally low strength, but some alluvial fan and alluvial plain sites also had extremely low strength.

Near-surface (3–15 cm [1–6 in.]) cone penetrometer measurements of the alluvial fan landform were significantly greater than those for all of the other landforms. The only other significant difference was between the alluvial plain and dune landforms, with the alluvial plain landform exhibiting the greater strength.

There were significant differences between landforms for all DCP indices except for the DCP initial depth metric (Figure 9). Dune DCP indices were significantly greater with two exceptions: (1) there was no significant difference with the sand sheet landform for any of the indices; and (2) there was no significant difference with the alluvial fan–sand sheet at a 15–30 cm (6 to 12 in.) depth. Sand sheet DCP indices were significantly greater than those for the alluvial fan but not the alluvial fan–sand sheet or alluvial plain landforms. Alluvial fan and alluvial plain DCP indices were among the lowest and were not significantly different from one another. Conversion of the DCP index to CBR using equations (3) and (4) has no effect on the results of these rank-based statistical comparisons. Overall, these comparisons show that dunes were significantly weaker through the full 1 m (39 in.) depth of the DCP than most of the other landforms and that alluvial fans were the strongest, especially at the surface.

Figure 9. Comparison of soil strength measurements with landform type. The *p*-values are Kruskal-Wallis one-way analysis of variance.

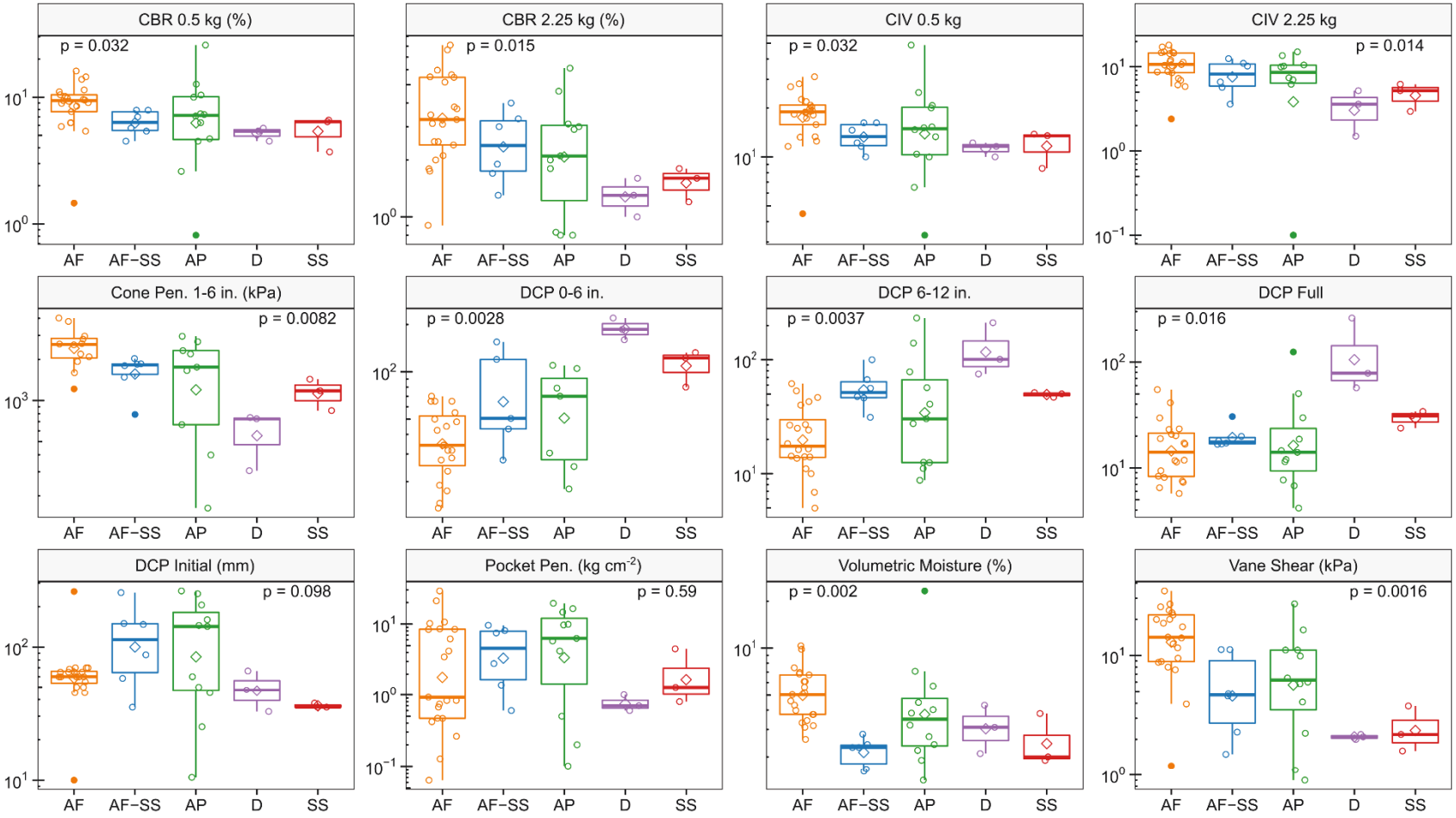

Table 6. Matrix of strength parameters showing significant difference between landform types based on $p < 0.05$ for both Conover and Iman (1979) and Kruskal-Wallis tests.

	AF	AF–SS	AP	D
AF-SS	CBR 0.5 kg; Clegg 0.5 kg; Cone Pen. 1–6 in.; DCP 6–12in.; Vol. Moist.; Vane Shear			
AP	CBR 2.25 kg; Cone Pen 1–6 in.; Vol. Moist.; Vane Shear	Vol. Moist.		
D	CBR 0.5 kg; CBR 2.25 kg; Clegg 0.5 kg; Clegg 2.25 kg; Cone Pen 1–6 in.; DCP 0–6 in.; DCP 6–12 in.; DCP Full; Vane Shear	DCP 0–6 in.; DCP Full	Cone Pen 1–6 in.; DCP 0–6 in.; DCP 6–12 in.; DCP Full	
SS	CBR 0.5 kg; CBR 2.25 kg; Clegg 0.5 kg; Clegg 2.25 kg; Cone Pen 1–6 in.; DCP 0–6 in.; DCP 6–12 in.; DCP Full; Vol. Moist.; Vane Shear	-	DCP Full	-

3.2 Cone penetrometer profiles

All of the cone penetrometer strength profiles indicated a weak surface layer over stronger soils at depth. This is typical of penetrometer profiles in natural soils where soils are generally more compacted and under increased confining stress with depth. The dune landform had consistently lower cone penetrometer values throughout the 0 to 460 mm (0–18 in.) soil depth profile compared with the other landforms (Figure 10). The alluvial landforms showed similar strength below 250 mm (10 in.) depth, while above this depth the sand sheet and the alluvial fan had the lowest and highest strength values, respectively. The typical strength characteristics of the sand sheet were a relatively thin low-strength layer overlying stronger alluvium, while the alluvial fan landform had a near-surface high strength layer to a depth of approximately 250 mm (10 in.) where it converged with

the other non-dune landforms. However, both the alluvial fan and alluvial plain landforms had very high variability between sites (Figure 11).

Figure 10. Mean cone penetrometer profiles for each landform.

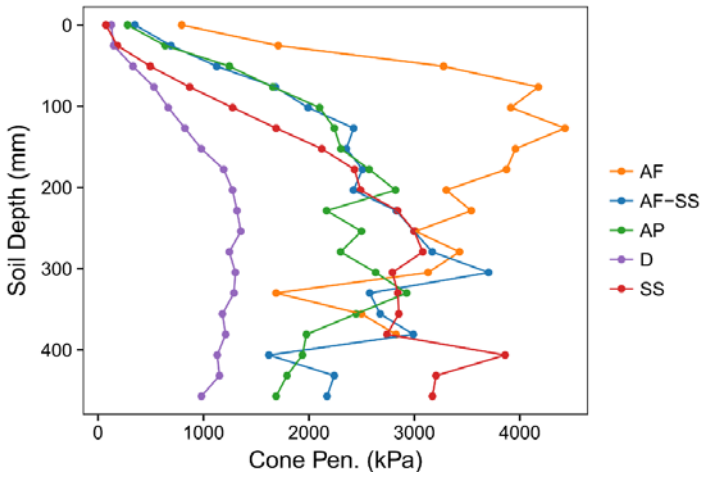

Figure 11. Mean cone penetrometer profiles for each landform. Shading is ±1 standard deviation.

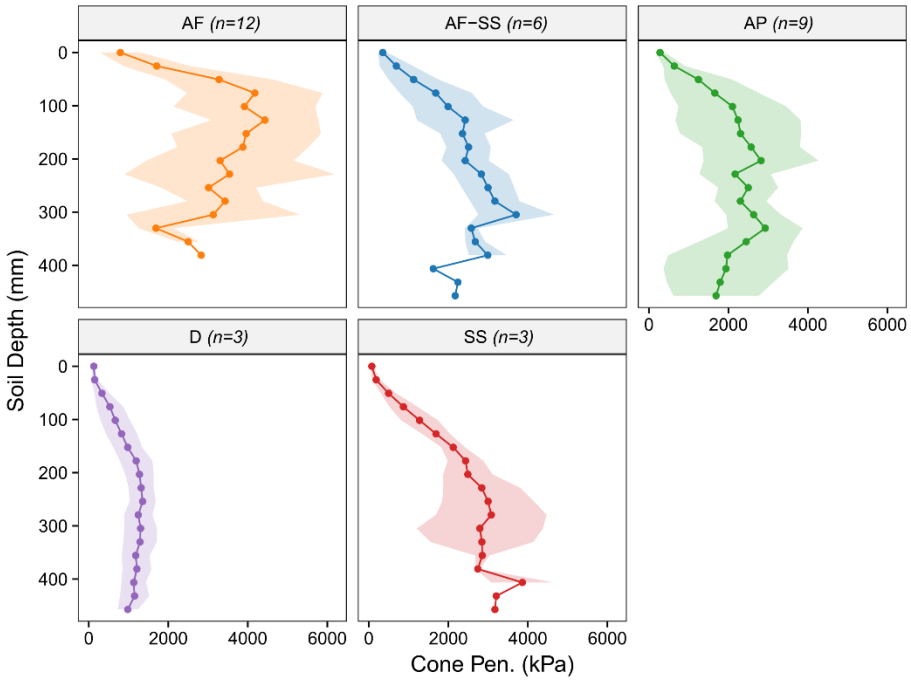

CBR values calculated from DCP depth profiles (Figure 12 and Figure 13) indicate that the dune and sand sheet landforms had generally lower strength through a depth of about 750 mm (30 in.) compared with the alluvial landforms. Although the alluvial fan–sand sheet landform had greater strength at the surface than the sand sheet landform, their

strengths converged at approximately a 600 mm (24 in.) depth. The alluvial fan landform had the greatest average strength within about the upper 300 mm (12 in.) but had roughly equivalent strength with the alluvial plain landform at depths greater than 375 mm (15 in.). Similar to the cone penetrometer profiles, the alluvial fan and alluvial plain landforms demonstrated the greatest variability in bearing capacity (CBR) as measured by the DCP (Figure 13).

Figure 12. Mean DCP CBR soil profiles by landform. Means are calculated on depth values rounded to 25 mm increments.

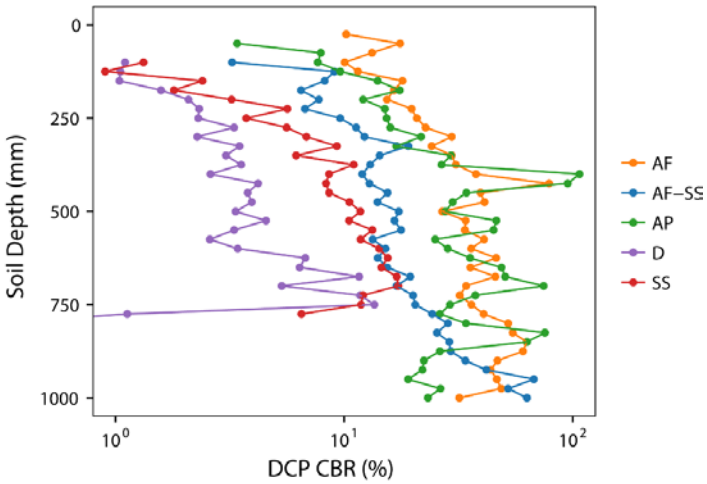

Figure 13. Mean DCP CBR soil profiles by landform. Means are calculated on depth values rounded to 25 mm increments. Shading represents minimum and maximum limits.

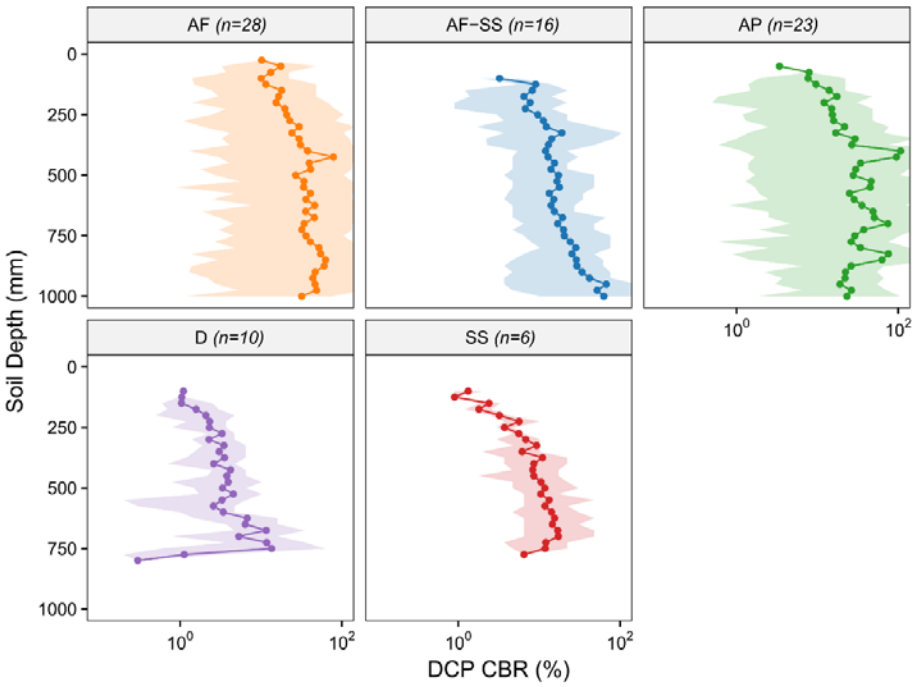

3.3 Soil strength relationships with surface soil composition

Sand and silt dominated the surface soil composition among sites. Dune and sand sheet landforms were firmly within USDA Sand classification whereas alluvial landforms extended into loamy sand, sandy loam, and silt loam (Figure 14). Calcium carbonate content typically ranged between less than 1% and 5%. LOI375 (a proxy for organic content) and gravimetric moisture were both typically less than 1%.

Figure 14. Ternary plot of <2 mm average surface soil texture based on USDA classes.

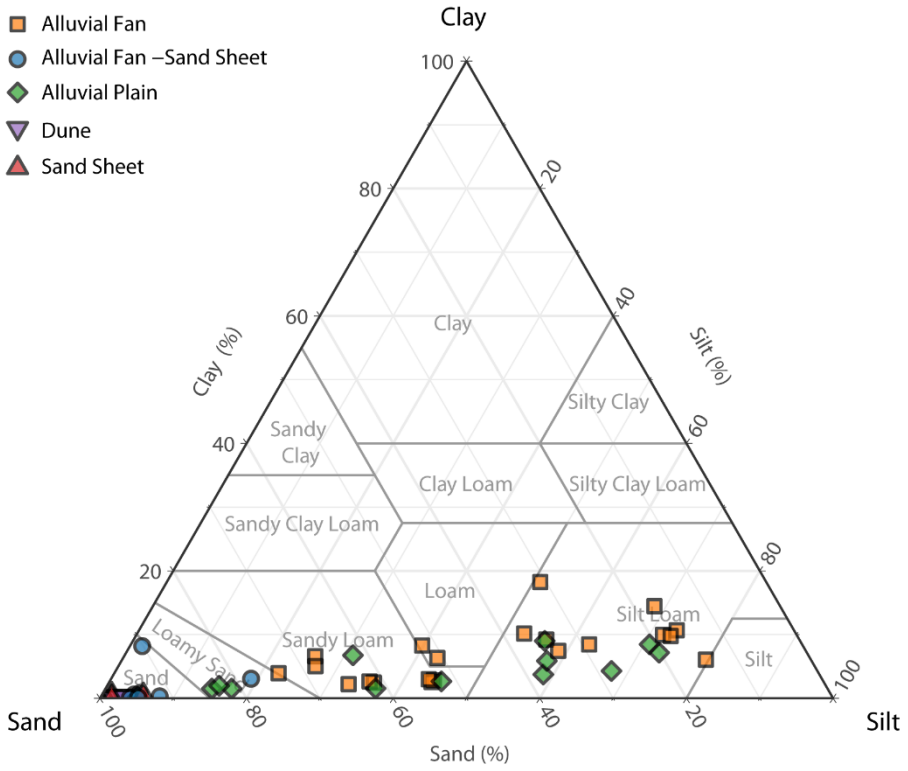

The soil bearing capacity metrics (i.e., Cleggs, cone penetrometer, and DCP indices) and vane shear were all significantly correlated with surface soil clay, silt, and sand percentages (Figure 15). In all cases, silt and clay were positively correlated with soil metrics indicative of stronger soil, whereas sand was negatively correlated with soil strength. The exception was the pocket penetrometer, which was uncorrelated with clay, silt, and sand. Volumetric moisture, gravimetric moisture, and organic content LOI375 were also significantly positively correlated with the bearing capacity and shear strength. Carbonate content was strongly negatively correlated with E-Gauge Density at 10 cm (4 in.) and uncorrelated with the other metrics.

The correlation of many soil composition metrics with each other made deducing the controlling variables difficult. For instance, soil moisture was strongly correlated with silt, clay, and LOI375, likely because finer-grain soils retain more water and allow vegetative growth because of high capillary forces.

Figure 15. Spearman correlation matrix of soil strength field measurements, surface soil composition lab measurements, PI-SWERL PM10 flux, and PI-SWERL threshold u^*. The p-values are noted as * <0.05, ** <0.01, and *** <0.001.

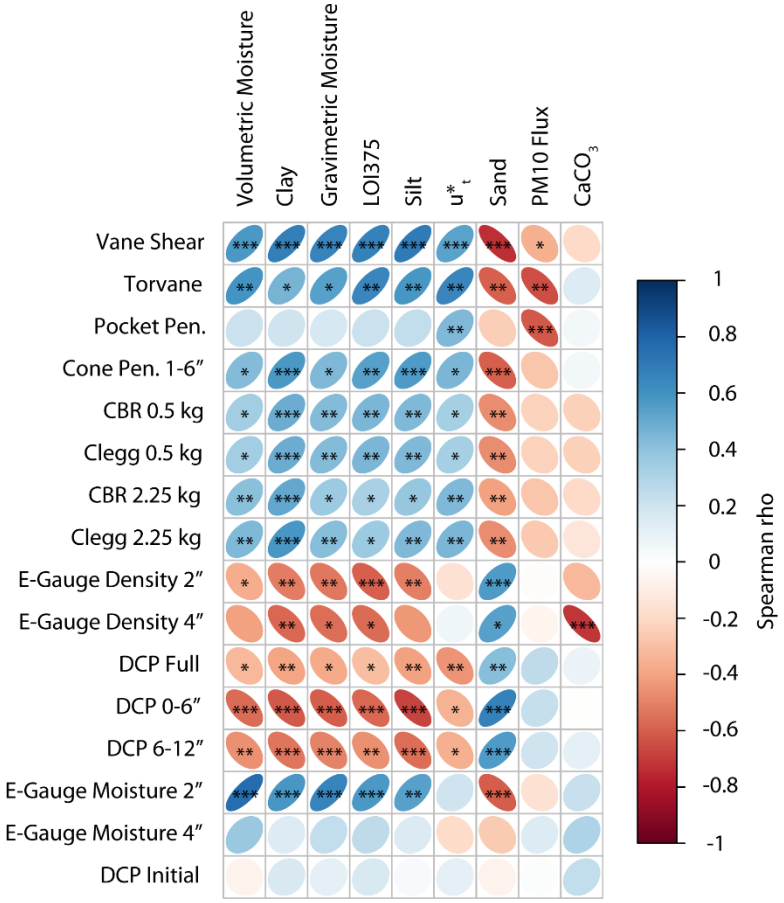

3.4 Soil strength relationships with dust emission

This study used two metrics of dust emission from the PI-SWERL. The first metric was estimated PM10 flux at an effective wind friction velocity (u^*) of 0.7 m s^{-1} (2.3 ft/s) which reflects the amount of dust produced from a surface. The second metric was the threshold wind friction velocity (u^*_t), which reflects the susceptibility of a surface to dust emission by saltation bombardment, the predominant mechanism for dust emission.

PM10 flux was significantly correlated only with the vane shear ($p < 0.05$), Torvane ($p < 0.01$), and pocket penetrometer ($p < 0.001$) (Figure 15). These measurements are all taken at or very near the soil surface. The correlations were all negative, indicating that stronger soils emit less dust. Simple linear regressions of these variables with PM10 flux yielded coefficients of determination (R^2) between 0.26 and 0.42 (Figure 16), which indicate only partial explanation of dust flux by each of these three different soil strength techniques. Multiple regression of all variables for just the PTD sites, where all variables were available, yielded an adjusted R^2 of 0.501. The lack of correlation with the other soil strength metrics likely reflects the soil depth at which these measurements were collected, with the vane shear, Torvane, and pocket penetrometer measuring the uppermost soil that is susceptible to dust emission.

Figure 16. Linear regression models for dust emission flux with vane shear (*left*), Torvane (*middle*; data available for PTD sites only), and pocket penetrometer (*right*).

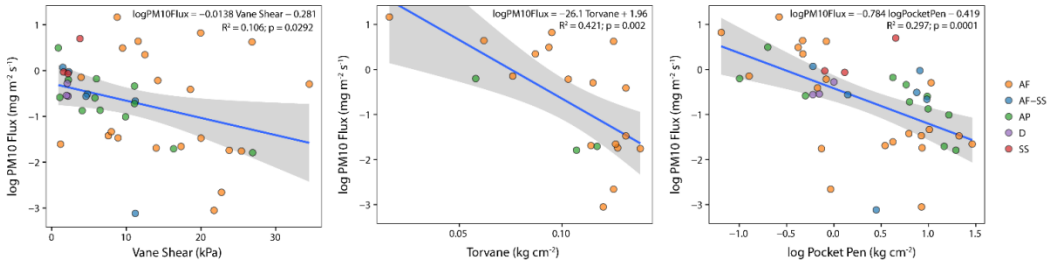

However, more soil strength metrics were significantly positively correlated with u^*_t: vane shear ($p < 0.001$), Torvane ($p < 0.01$), pocket penetrometer ($p < 0.01$), cone penetrometer ($p < 0.05$), 0.5 kg CIV and CBR ($p < 0.05$), and 2.25 kg CIV and CBR ($p < 0.01$) (Figure 15). All DCP indices, which are inversely related to bearing capacity, were significantly negatively correlated with u^*_t ($p < 0.05$), consistent with the theme of stronger soil requiring greater wind friction velocities for dust emission. The correlation with subsurface measurements, such as the cone penetrometer and full DCP index, highlights the importance of full soil profile strength on susceptibility to dust emission. The finding of a positive relationship between u^*_t and the pocket penetrometer is similar to that found by Li et al. (2010) using a wind tunnel in the Mojave Desert and to that found by Bacon et al. (2011) using a PI-SWERL in the Negev Desert of Israel. However, linear regressions of the surface soil strength metrics with u^*_t (Figure 17) yielded R^2 values of 0.26, 0.31, 0.16, and 0.12 for the vane shear, Torvane, pocket penetrometer, and CBR 2.25 kg, respectively. These relatively low

coefficients indicate only partial explanation of the susceptibility for dust emission by these soil strength metrics.

Figure 17. Linear regression models for threshold friction velocity with select surface soil strength metrics. Torvane data are available for only PTD sites.

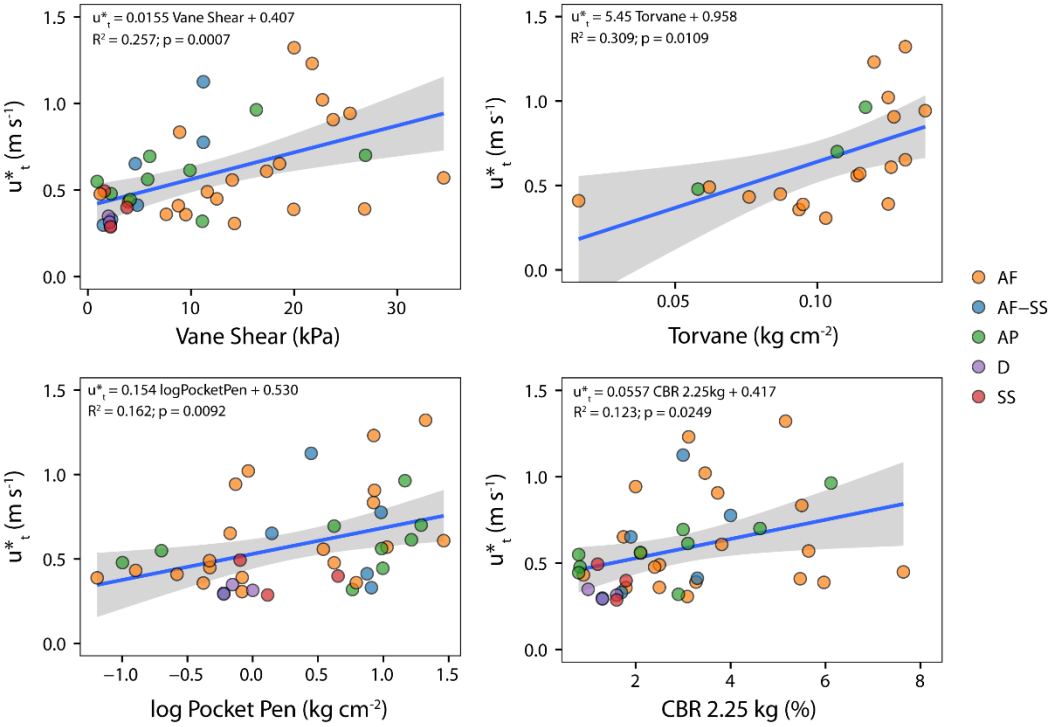

4 Conclusions and Recommendations for Future Work

This initial work in the U.S. desert southwest indicates that soil bearing capacity and shear strength vary with geomorphic landform type, likely reflecting alluvial and aeolian controls on soil texture, composition, and development. From this analysis, we concluded the following:

- The aeolian landforms—dune and sand sheet—tended to have significantly lower bearing capacity and shear strength than the alluvial landforms.
- Overall, surface soil silt and clay contents were positively correlated, and sand content negatively correlated, with soil strength parameters.
- The alluvial fan and alluvial plain landforms had the greatest soil strength and a greater proportion of silt and clay than the other sand-dominated landforms.
- Increased bearing capacity and shear strength at the soil surface was significantly associated with decreased dust emission fluxes and increased wind velocities to initiate emission.
- Dunes were significantly weaker through the full 1 m (39 in.) depth of the DCP than most of the other landforms; and alluvial fans were the strongest, especially at the surface.
- The dune landform had consistently lower cone penetrometer values throughout the 0 to 460 mm (0–18 in.) soil depth profile compared with the other landforms.

Collecting data from more sites within each studied landform and from other landforms (e.g., playas, pavements, loess fields, floodplains, deltas, hillslopes, and periglacial environments) would improve the statistical power and understanding of geomorphological controls on soil strength and dust emission. In addition, the temporal variability of the observed relationships should be explored by testing across seasons. Additional variables that may more completely explain soil strength should be assessed in

future research efforts, including the effects of aspect, wind direction, and sediment provenance, which is associated with grain shape and composition. Biological processes also have an important role through the development of biocrusts, vegetative bioirrigation, and faunal burrowing. The latter caused at least two erratic DCP measurements during the field study and may have a significant role in overall soil strength.

All of the sites investigated in this project had very low vegetation. Vegetative effects may confound the relationships, but the impact of vegetation is critical. Other work has indicated the need for future work in this area, especially with regard to quantifying how vegetation impacts the strength of the soil in a way that is applicable to predicting vehicle mobility (Wieder and Shoop 2017).

Response to disturbance was only minimally addressed in this study, yet it is an important variable in soil strength and dust emission. The soils examined in this study were either in their natural state or undisturbed by humans in recent time (>10–25 years). Disturbance by agriculture, marching, vehicles (wheeled and tracked), rotorwash, and fire likely affects soil strength differently across landform types. Fugitive dust emissions from these different disturbance modes may also vary significantly between landform types but have not yet been fully studied within this research area. While some disturbance measurements were taken for this study, none were analyzed in this report, and the impact of disturbance and fugitive dust is an important area of future work.

As researchers generate geomorphological and soil strength maps by using remote sensing and other methods, there is a need to validate soil strength estimates in the field. Geospatial products will need to be validated across a wide range of landform types and regions. Ongoing soil strength studies such as those on Department of Defense installations (i.e., Yuma Proving Ground, Holloman Air Force Base, Fort Hunter Liggett, and Fort Bliss) could be leveraged to validate and improve future map-based soil strength predictions.

References

AMS. 2018. Part #59035 GeoTester Penetrometer Technical Data Sheet. American Falls, ID: AMS, Inc. http://www.ams-samplers.com/pdfs/ams-Geotester-Without-price.pdf.

ASABE (American Society of Agricultural and Biological Engineers). 2006a. *Soil Cone Penetrometer*. ASAE S313.3 FEB04. St. Joseph, MI: American Society of Agricultural and Biological Engineers.

———. 2006b. *Procedures for Using and Reporting Data Obtained with the Soil Cone Penetrometer*. ASAE EP542 FEB99. St. Joseph, MI: American Society of Agricultural and Biological Engineers.

ASTM. 2015. *Standard Test Method for Use of the Dynamic Cone Penetrometer in Shallow Pavement Applications*. ASTM D6951/D6951M-09. West Conshohocken, PA: ASTM International. www.astm.org.

———. 2016. *Standard Test Methods for Determination of the Impact Value (IV) of a Soil*. ASTM D5874-16. Conshohocken, PA: ASTM International. www.astm.org.

Bacon, S. N., E. V. McDonald. 2016. Regional Distribution of Salt-Rich Dust Across Southwest Asia Based on Predictive Soil-Geomorphic Mapping Techniques. In *Military Geosciences and Desert Warfare*, ed. E. V. McDonald and T. Bullard, 237–256. New York: Springer New York.

Bacon, S. N., E. V. McDonald, R. Amit, Y. Enzel, and O. Crouvi. 2011. Total Suspended Particulate Matter Emissions at High Friction Velocities from Desert Landforms. *Journal of Geophysical Research* 166:F03019.

Berney, E. S., M. Mejías-Santiago, and M. D. Norris. 2016. *Validation Testing of Non-Nuclear Alternatives to Measuring Soil Density*. ERDC/GSL TR-16-28. Vicksburg, MS: U.S. Army Engineer Research and Development Center.

Bullard, J. E., S. P. Harrison, M. C. Baddock, N. Drake, T. E. Gill, G. McTainsh, and Y. Sun. 2011. Preferential Dust Sources: A Geomorphological Classification Designed for Use in Global Dust-Cycle Models. *Journal of Geophysical Research: Earth Surfaces* 116 (F4): F04034.

Clegg, B. 1980. An Impact Soil Test as Alternative to California Bearing Ratio. In *Proceedings, 3rd Australian-New Zealand (ANZ) Geomechanics Conference*, Wellington, New Zealand, 1:225–230.

Conover, W. J., and R. L. Iman. 1979. *On Multiple-Comparisons Procedures*. LA-7677-MS. Los Alamos, NM: Los Alamos Scientific Laboratory.

Etyemezian, V., G. Nikolich, S. Ahonen, M. Pitchford, M. Sweeney, R. Purcell, J. Gillies, and K. Kuhns. 2007. The Portable In Situ Wind Erosion Laboratory (PI-SWERL): A New Method to Measure PM10 Windblown Dust Properties and Potential for Emissions. *Atmospheric Environment* 41:3789–3796.

Etyemezian, V., J. A. Gillies, M. Shinoda, G. Nikolich, J. King, and A. R. Bardis. 2014. Accounting for Surface Roughness on Measurements Conducted with PI-SWERL: Evaluation of a Subjective Visual Approach and a Photogrammetric Technique. *Aeolian Research* 13:35–50.

García-Gaines, R. A., and S. Frankenstein. 2015. *USCS and the USDA Soil Classification System*. ERDC/CRREL TR-15-4. Hanover, NH: U.S. Army Engineer Research and Development Center.

Li, J., G. S. Okin, J. E. Herrick, J. Belnap, S. M. Munson, and M. E. Miller. 2010. A Simple Method to Estimate Threshold Friction Velocity of Wind Erosion in the Field. *Geophysical Research Letters* 37:L10402.

McDonald, E., S. Bacon, S. Baker, R. Amit, J. L. Antinao, M. Berli, T. Bullard, T. Caldwell, O. Crouvi, Y. Enzel, H. Green, F. Iwashita, D. Koracin, J. D. McAlpine, T. Minor, N. Regmi, and D. Sabol. 2013. *Integrated Desert Terrain Forecasting for Military Operations*. Reno, NV: Desert Research Institute.

McDonald, E. V., K. Adams, and M. R. Sweeney. 2018. *Great Basin Cooperative Ecosystem Studies Unit (GBCESU): Collaborative Project to Assess Regional Soil Dust Emission for Select Areas of the SW US Deserts*. Final project report submitted to U.S. Army Engineer Research and Development Center (ERDC), Cold Regions Research and Engineering Laboratory. Reno, NV: Desert Research Institute.

Millar, L. R. 1977. Application of the Soil Impact Tester to Road Pavement Construction. Honours Thesis, Department of Civil Engineering, University of Western Australia, Crawley, Western Australia.

Parajuli, S. P., and C. S. Zender. 2017. Connecting Geomorphology to Dust Emission through High-Resolution Mapping of Global Land Cover and Sediment Supply. *Aeolian Research* 27:47–65.

R Core Team. 2017. *R: A Language and Environment for Statistical Computing*. Vienna, Austria: R Foundation for Statistical Computing. https://www.R-project.org/.

Shoop, S. A., J. Crandell, and M. Knuth. 2012. Using a Clegg Impact Hammer to Measure Snow Strength. In *Proceeding of the 15th International Conference on Cold Regions Engineering*, Quebec, Canada, 19–22 August, 811–822.

Sopher, A. M., S. A. Shoop, J. M. Stanley, and B. T. Tracy. 2016a. *Image Analysis and Classification Based on Soil Strength*. ERDC/CRREL TR-16-13. Hanover, NH: U.S. Army Engineer Research and Development Center.

———. 2016b. Image Analysis and Classification Based on Soil Strength. In *Proceedings, 8th Americas Conference of the International Society for Terrain Vehicle Systems (ISTVS)*, 12–14 September, Detroit, MI, paper number 98. https://www.istvs.org/proceedings-orders/8th-north-american-conf-2016-detroit.

Spectrum Technologies. 2013. *Field Scout SC 900 Soil Compaction Meter Product Manual*. Aurora, IL: Spectrum Technologies, Inc.

U.S. Army. 1994. *Planning and Design of Roads, Airfield, and Heliports in the Theater of Operations—Road Design*. FM 5-430-00-1. Washington, DC: Headquarters, Department of the Army.

Wieder, W. L., and S. A. Shoop. 2017. *Vegetation Impact on Soil Strength: A State of the Knowledge Review*. ERDC/CRREL SR 17-2. Hanover, NH: U.S. Army Engineer Research and Development Center.

Yoder, E. J., and M. W. Witczak. 1975. *Principles of Pavement Design*. 2nd ed. New York: John Wiley and Sons, Inc.

Appendix A: Supplementary Graphical Data

Figure A-1. Average cone penetrometer depth profiles for each site.

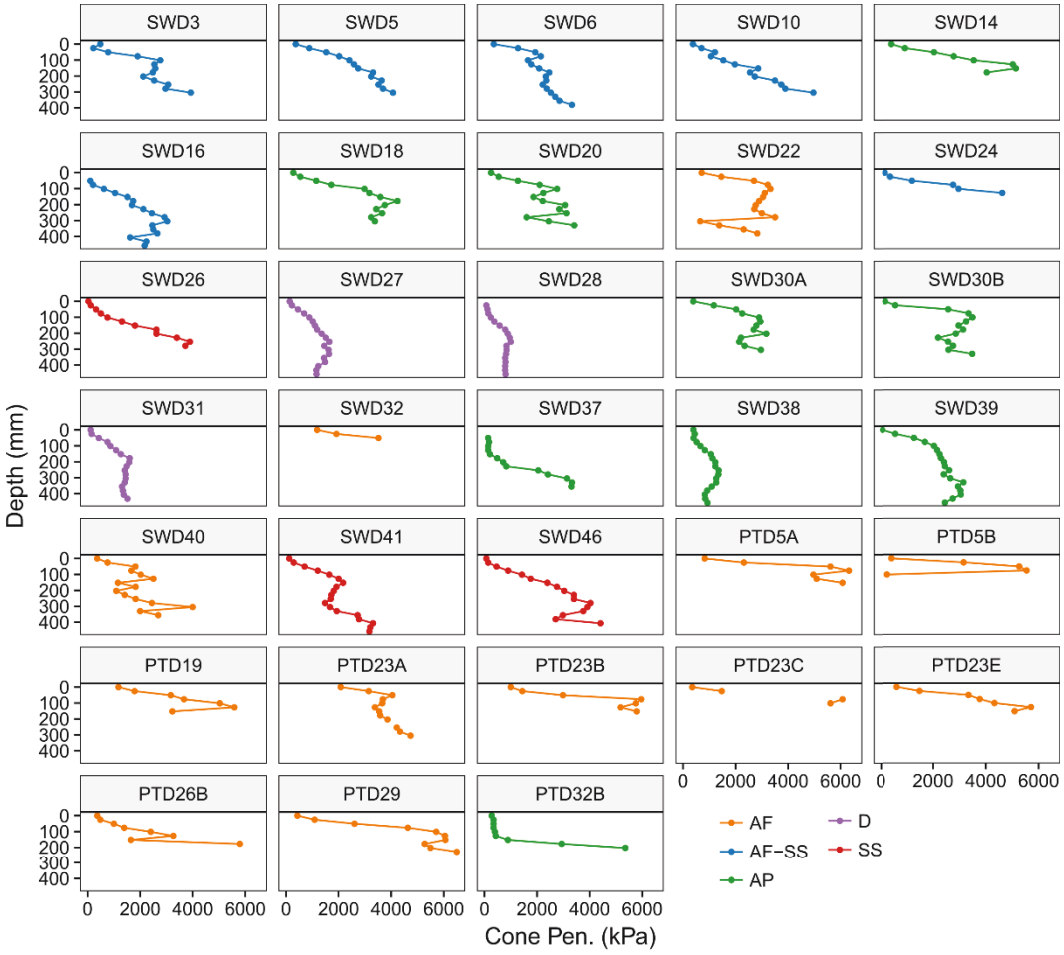

Figure A-2. DCP CBR soil profiles for each site.

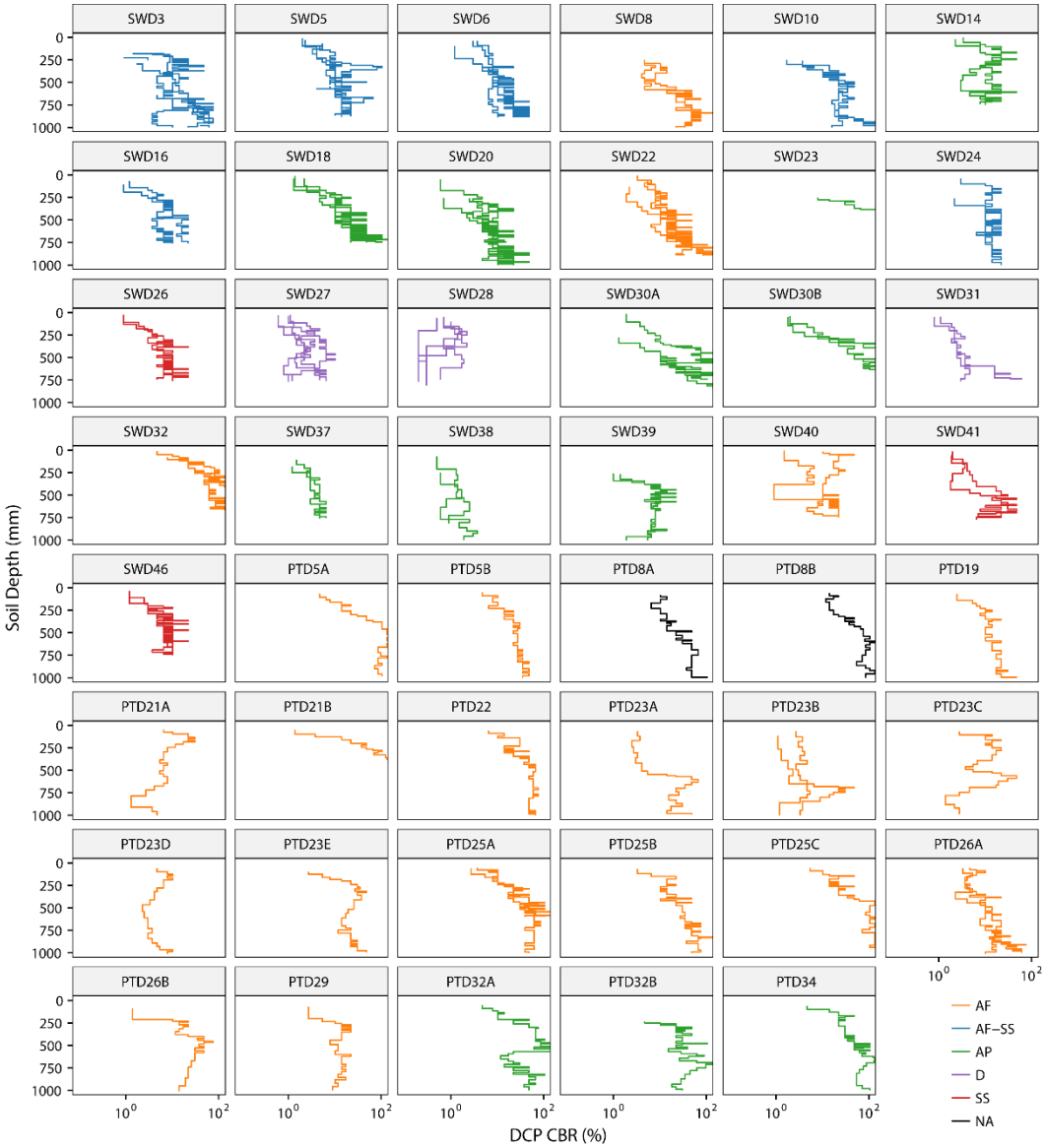

Figure A-3. Spearman correlation matrix of soil strength field measurements, PI-SWERL PM10 flux, PI-SWERL threshold u^*, and surface soil composition lab measurements for all sites. The p-values are noted as * < 0.05, ** < 0.01, and *** <0.001.

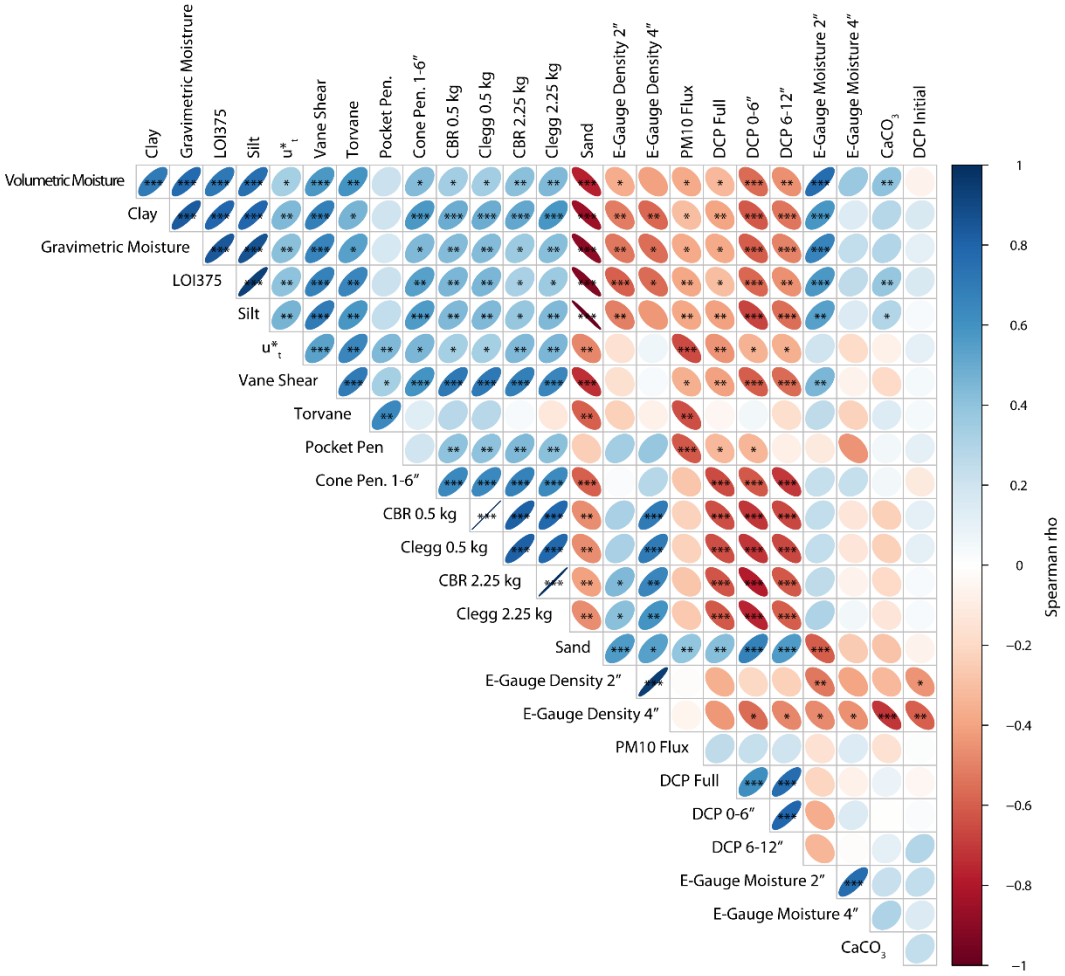

Appendix B: Tabular Soil Strength Data

Table B-1. Averaged soil strength data used in this study. Density is abbreviated as *dens.* and moisture as *moist.* Undisturbed (*undist.*) and disturbed (*dist.*) values are specified for some measurements taken before and after disturbance by hand raking and boot shuffling, respectively.

	Clegg			E-Gauge					Pocket Pen.				Torvane (kg cm^{-2})		DCP			
Site	2.25 kg	0.5 kg	0.5 kg Dist.	Dens. 2 in. (lb ft^{-3})	Dens. 4 in. (lb ft^{-3})	Moist. 2 in. (%)	Moist. 4 in. (%)	Vol. Mois. (%)	Undist.	Dist.	Vane Shear (kPa)	Cone Pen 1–6 in. (psi)	Undist.	Dist.	Initial Depth (mm)	0–6 in. Index	6–12 in. Index	Full Depth Index
SWD3	12.5	14.6	16.6	–	–	–	–	1.7	9.6	0.2	11.2	261	–	–	147.5	120.0	66.9	17.2
SWD5	10.2	12.2	14.7	–	–	–	–	2.3	2.8	2.8	11.2	294	–	–	35.0	50.6	31.3	18.0
SWD6	6.6	11.6	11.1	–	–	–	–	2.4	1.4	0.9	4.6	267	–	–	58.3	43.3	46.2	19.9
SWD8	18.1	18.9	14.2	100.4	–	2.7	–	6.1	10.2	0.6	8	–	–	–	260.0	–	40.0	11.8
SWD10	5.7	16.2	–	–	–	–	–	2.3	8.1	–	2.3	215	–	–	255.0	–	100.0	16.7
SWD14	10	15.1	–	88.3	–	3.9	–	7.1	5.8	–	11.1	429	–	–	10.5	30.5	12.6	18.7
SWD16	3.6	10.0	–	–	–	–	–	1.6	0.6	–	1.5	115	–	–	87.5	155.0	56.2	30.6
SWD18	7.4	15.3	12.7	94.5	–	1.4	–	3.2	9.7	0.8	5.8	318	–	–	25.0	105.0	40.8	14.0
SWD20	10.5	13.3	12.9	91.8	–	3.9	–	5.7	16.4	0.9	9.9	255	–	–	206.3	–	56.9	14.6
SWD22	15.1	13.3	11.5	–	–	–	–	5.6	8.4	1.3	8.9	408	–	–	68.3	34.2	42.9	17.2
SWD23	–	48.7	–	–	–	–	–	2.7	–	–	6.5	–	–	–	250.0	–	12.5	4.2
SWD24	11	16.2	10.4	–	–	–	–	2.8	7.5	0.3	4.8	269	–	–	150.0	27.5	47.5	16.8
SWD26	2.95	8.5	–	–	–	–	–	3.8	0.8	–	1.6	122	–	–	35.0	132.5	51.4	34.2
SWD27	3.6	11.6	–	–	–	–	–	4.3	0.6	–	2.2	109	–	–	32.5	186.3	100.9	78.5
SWD28	1.5	10.0	–	–	–	–	–	3.1	0.7	–	2	44	–	–	66.3	220.0	211.5	261.2
SWD30A	10.2	20.0	–	–	–	–	–	1.9	4.2	–	6	337	–	–	145.0	70.0	27.5	12.0
SWD30B	6.2	10.4	15.8	94.0	–	1.4	–	2.4	0.5	0.4	1.1	391	–	–	45.0	78.8	30.3	11.5
SWD31	5.2	12.2	–	–	–	–	–	2.1	1	–	2.1	107	–	–	47.5	160.0	75.0	57.1
SWD32	8.5	15.8	13.6	96.7	–	2.7	–	6.1	4.2	4.2	1.2	371	–	–	45.0	13.6	5.0	5.7
SWD37	0.1	6.5	–	86.2	–	1.8	–	1.4	0.2	–	0.9	24	–	–	142.5	110.0	78.3	50.4
SWD38	0.1	10.0	11.1	87.8	–	1.5	–	2.2	9.9	0.8	4.1	97	–	–	160.0	–	232.5	124.6
SWD39	7	14.7	10	74.6	–	7.0	–	23.3	6.3	2.1	11.1	241	–	–	262.5	–	140.0	29.8
SWD40	8.8	11.6	17.1	99.6	–	2.1	–	4.3	6.2	0.7	7.6	232	–	–	10.0	48.1	25.0	23.4
SWD41	6.2	13.5	8.5	97.7	–	0.9	–	2.0	4.5	0.3	3.8	208	–	–	35.0	80.0	46.9	23.8
SWD46	5.2	13.8	–	–	–	–	–	1.9	1.3	–	2.2	171	–	–	37.5	122.5	50.2	31.0
PTD5A	10.5	21.9	–	85.3	88.9	8.7	8.8	10.4	8.44	0.06	21.8	584	0.12	0.02	65.0	31.7	14.0	7.5

Table B-1 (cont.). Averaged soil strength data used in this study. Density is abbreviated as *dens.* and moisture as *moist.* Undisturbed (*undist.*) and disturbed (*dist.*) values are specified for some measurements taken before and after disturbance by hand raking and boot shuffling, respectively.

	Clegg			E-Gauge					Pocket Pen.				Torvane (kg cm^{-2})		DCP			
Site	2.25 kg	0.5 kg	0.5 kg Dist.	Dens. 2 in. (lb ft^{-3})	Dens. 4 in. (lb ft^{-3})	Moist. 2 in. (%)	Moist. 4 in. (%)	Vol. Mois. (%)	Undist.	Dist.	Vane Shear (kPa)	Cone Pen 1–6 in. (psi)	Undist.	Dist.	Initial Depth (mm)	0–6 in. Index	6–12 in. Index	Full Depth Index
PTD5B	14.6	20.8	–	88.2	91.2	2.6	2.7	9.8	10.66	0.10	34.5	303	0.115	0.018	50.0	27.5	18.3	11.4
PTD8A	20.9	33.2	–	102.2	104.0	3.4	3.6	5.6	6.93	0.07	37.0	–	0.099	0.014	80.0	17.5	22.1	10.6
PTD8B	21.2	28.8	–	100.5	105.6	8.3	9.6	10.7	0.33	–	46.5	–	0.016	0.016	60.0	14.0	14.6	6.3
PTD19	6.9	18.1	–	75.6	80.6	4.4	2.7	7.5	0.74	0.13	25.4	318	0.138	0.02	70.0	70.0	24.2	16.8
PTD21A	17.2	22.6	–	94.3	101.7	2.9	2.5	3.1	0.47	0.05	12.5	–	0.087	0.021	45.0	14.6	16.3	29.7
PTD21B	11.6	19.7	–	89.4	93.5	5.0	3.0	7.0	8.55	0.09	23.8	–	0.127	0.021	50.0	31.7	6.9	8.3
PTD22	14.4	27.0	–	90.7	97.9	3.0	2.3	5.2	21.05	0.09	20.0	–	0.131	0.019	60.0	17.5	10.0	7.3
PTD23A	7.3	18.3	–	84.5	84.7	2.2	2.5	3.8	3.47	0.04	14.0	379	0.114	0.02	65.0	55.0	61.7	23.1
PTD23B	6.1	12.5	–	81.7	83.1	3.2	2.8	3.4	0.42	0.03	9.5	430	0.0936	0.019	65.0	65.0	53.3	55.0
PTD23C	10.7	19.1	–	81.2	81.0	3.2	2.8	6.8	0.83	0.09	26.8	280	0.125	0.02	70.0	23.3	14.3	20.2
PTD23D	11.3	19.3	–	81.1	86.3	3.9	3.5	6.7	0.92	0.05	22.8	–	0.125	0.021	60.0	28.3	27.0	41.3
PTD23E	5.8	13.2	–	81.1	85.9	3.2	2.4	4.6	0.67	0.07	18.6	376	0.131	0.017	60.0	65.0	14.1	11.7
PTD25A	14.9	18.7	–	89.5	93.3	3.7	3.5	4.0	0.26	0.21	8.8	–	0.016	0.01	60.0	50.0	16.5	8.1
PTD25B	10.4	20.3	–	93.2	100.3	2.9	2.8	2.6	0.83	0.05	14.2	–	0.103	0.016	65.0	42.5	13.6	9.4
PTD25C	14.7	31.1	–	96.9	97.5	4.0	4.0	5.0	0.06	0.06	20.0	–	0.095	0.011	55.0	19.0	11.0	6.5
PTD26A	12.0	28.2	–	101.8	102.7	2.2	2.2	3.8	28.96	0.08	17.3	–	0.126	0.013	60.0	45.0	46.7	20.8
PTD26B	2.4	4.5	–	90.7	94.2	2.3	2.3	3.2	0.13	0.11	4.0	176	0.076	0.014	–	–	–	–
PTD29	8.7	17.3	–	92.7	91.3	2.2	2.7	3.3	0.47	–	11.6	551	0.062	0.016	70.0	65.0	26.7	18.9
PTD32A	15.1	20.7	–	97.0	100.8	2.9	2.6	4.0	14.64	0.08	16.3	–	0.117	0.015	50.0	25.0	11.1	7.7
PTD32B	–	3.3	–	79.5	80.1	3.8	3.8	4.5	0.10	0.06	2.3	58	0.058	0.014	–	–	–	–
PTD34	13.6	24.9	–	100.9	103.7	1.9	1.7	3.8	19.47	0.12	26.9	–	0.107	0.016	60.0	18.0	8.8	6.8

Table B-2. Clegg data for the PTD sites.

Site	Flag #	0.5 kg Clegg				2.25 kg Clegg			
		Drop 1	Drop 2	Drop 3	Drop 4	Drop 1	Drop 2	Drop 3	Drop 4
PTD5A	1	11.6	15	17.8	19.1	6.2	11	11	11.3
	2	11.5	16.2	19.8	19.3	4.6	7.6	8.5	9.2
	3	13.3	19.2	20.9	23.1	6.7	9.7	10.6	11
	4	12.7	18.6	23.7	26.1	10.8	12.2	11.7	11.5
PTD5B	1	14.5	18.8	20.3	19.2	11.9	13.1	14.9	15.6
	2	17.2	20.1	21.7	22	10.6	11.9	11.9	12
	3	14.4	17.4	17.5	18.5	10.6	9.7	11.7	12
	4	17.1	21	22.9	23.6	14	18.6	19.7	21.3
PTD8A	1	16.5	27.7	33.3	35.5	11.3	18.1	20.2	20.4
	2	26.4	35.2	36.1	34.4	23.6	26.4	24.1	24.3
	3	18.8	28.8	31.7	35.3	16.5	18.8	19.3	19
	4	17.1	22.2	26.2	27.4	17.9	19.1	19.9	19.1
PTD8B	1	8.5	13.4	17.1	19.2	12.4	14.2	16.3	16.7
	2	29.4	28.9	28.9	31.1	27.7	27.1	27.7	28.9
	3	18.5	26.3	28.1	27.2	17	18.4	18.4	18.6
	4	21.3	28.4	32.9	37.6	18.4	19.9	22.5	22.7
PTD19	1	12.5	18.6	20	20.4	5.8	7.1	7.8	8.7
	2	10.3	15.1	15.5	15.8	4.6	6.5	7.6	7.9
	3	14.3	18.4	20.1	20.2	5.8	7.2	7.6	7.9
	4	12.9	15.3	15.4	15.9	4.7	4.6	4.6	5.8
PTD21A	1	10.6	14.8	18.6	20	9.4	11.7	13.3	15.2
	2	15.5	21.8	23.7	24.3	15.4	19.1	20.9	22.2
	3	11.7	16.5	18.5	19.8	12.4	14.9	16.5	17.5
	4	14.6	21.2	25.5	26.2	14.5	17.4	18.1	19
PTD21B	1	14.1	19	22.4	23.1	10.6	14.3	14.9	15.2
	2	13.1	16.9	16.8	19.1	9.7	11.9	11.5	11.7
	3	11.9	16.2	18	18.1	7.8	7.8	7.6	7.8
	4	10.8	15	17.5	18.4	11.1	13.6	12.2	13.5
PTD22	1	14	28.5	34.9	37.2	8.5	12.2	14	16.3
	2	15.3	20.8	21.7	23.6	8.8	10.8	12.2	12.2
	3	14.6	20.1	21.1	22.2	12.9	17.4	17	18.4
	4	12.5	20	23.1	25	12.2	14.9	14.2	14.7
PTD23A	1	12.3	17.8	19	20.4	2.8	5.1	5.5	6.2
	2	8.8	13.6	15.3	15.5	6.7	8.3	9.7	8.7
	3	9.8	15.1	16.8	17.3	5.6	6.7	6.7	7.6
	4	8.2	15.2	17.5	20	6	6.9	7.2	6.7

Table B-2 (cont.). Clegg data for the PTD sites.

Site	Flag #	0.5 kg Clegg				2.25 kg Clegg			
		Drop 1	Drop 2	Drop 3	Drop 4	Drop 1	Drop 2	Drop 3	Drop 4
PTD23B	1	10.2	9.6	10.5	9.6	3.3	4.6	5.6	5.5
	2	13.2	15.5	16.4	16.6	4.2	4.9	5.6	6.5
	3	11.4	12.2	12.2	11.9	3.9	5.1	5.6	6.7
	4	7.1	10.5	11.8	11.9	4.7	6.5	7.6	8.8
PTD23C	1	11.9	17.8	18.3	20	8.5	12.2	12.7	13.5
	2	14.6	18.8	17.6	18.3	9.4	11	12	11.9
	3	15.4	21.4	22.6	21.8	9.4	10.6	10.8	11
	4	12	14.7	16.2	16.2	5.6	6.9	7.1	7.4
PTD23D	1	11.2	14.3	16.2	17.9	6.3	10.6	11.9	13.3
	2	12.8	16	16.3	19.9	5.5	9.4	11.9	11.9
	3	6.2	12.6	14.4	16.7	6.7	10.1	12	11.7
	4	15.1	16.8	20.1	22.5	7.4	8.8	9.4	9
PTD23E	1	9.6	11.6	13.1	12.2	3.3	4.9	4.2	7.1
	2	13.2	14.3	13.4	12.6	4	4	5.5	5.1
	3	13.5	14.6	13.4	15.4	6.7	5.8	7.6	8.5
	4	11.9	12.6	12.4	12.7	4.4	5.8	6	6.9
PTD25A	1	10.9	12.9	13.7	15.2	9.7	11.9	13.3	14
	2	20.9	19.1	21.5	22.8	11.9	16.1	17	17.9
	3	16.7	16.7	16.6	16	11.1	13.6	14	14.7
	4	13.2	17.3	20.8	20.8	12	15.6	15.2	17
PTD25B	1	13	18.5	19.4	20.8	9	14	12.6	12.7
	2	18.5	24.3	22.5	21.1	7.6	9	9.7	9.9
	3	17.9	19.9	18.1	14.7	18.3	9.9	9.7	11
	4	19.4	24.1	25.6	24.6	10.3	10.4	9.4	10.4
PTD25C	1	15.5	27.4	29.5	32	5.8	7.9	8.7	9.7
	2	17.5	22.1	22.3	22.7	13.8	16.7	14.5	14.5
	3	27.2	32.8	34	34.2	17.2	18.6	20.2	18.6
	4	23.5	31.9	34.3	35.5	12.9	15.1	15.4	16.5
PTD26A	1	17.3	28.7	29.4	30.1	9	12.7	12.4	12
	2	16.8	25.8	30	29.6	11.3	13.1	13.3	14.2
	3	13.5	19.2	22.2	23.5	11.9	11	9.7	8.3
	4	18.9	25.6	26.8	29.4	10.8	13.6	12.7	12.4
PTD26B	1	2.7	3.7	4.3	3.9	0	0	2.4	2.8
	2	7.1	8	8	5.5	0	0	0	0
	3	2.1	3	3.1	3.5	0	0	0	0
	4	4.7	4.4	4.3	5	0	0	0	2.6

Table B-2 (cont.). Clegg data for the PTD sites.

Site	Flag #	0.5 kg Clegg				2.25 kg Clegg			
		Drop 1	Drop 2	Drop 3	Drop 4	Drop 1	Drop 2	Drop 3	Drop 4
PTD29	1	18.5	16	20.6	18.6	6.2	8.8	9	8.8
	2	13.1	13.2	12.8	14.8	9	7.9	7.4	8.8
	3	17	12.9	13.8	15	6	8.1	9.4	10.3
	4	16.1	16.6	19.2	19.8	4.9	4.9	6.5	6.9
	5	12.6	14.3	13.4	15.5	7.8	8.8	10.1	9.4
	6	17	19.4	20.7	20	6.3	8.5	9.7	9.9
PTD32A	1	13.9	18.6	18.3	19.6	6.5	9	12.4	13.6
	2	14.3	18.7	22.6	22.7	10.8	15.9	18.1	20.4
	3	9.9	12.7	13.2	14.4	6.2	8.8	10.4	11.7
	4	17.1	24.1	26.4	26.2	12.6	17.2	19.3	20
PTD32B	1	4.9	3.5	3.5	3.3	0	0	0	0
	2	3.7	4.7	4.9	3.3				
	3	7.1	3.7	3.4	3.1				
	4	4.3	3.4	2.6	3.5	0	2.4	0	0
PTD34	1	15.7	17.9	22.1	23.1	8.7	11.9	12.2	14
	2	25.8	26.8	26.3	27	7.2	11.3	13.1	15.4
	3	23.1	32.4	33.1	29.9	9.2	13.3	15.4	16.8
	4	11.3	16.1	17.1	19.5	8.3	12	13.6	15.4

Table B-3. Average Clegg data for the SWD sites.

Site	3rd drop 2.25 kg Clegg Undisturbed	4th drop 0.5 kg Clegg Undisturbed	4th drop 0.5 kg Clegg Disturbed
SWD3	12.5	14.6	16.6
SWD5	10.2	12.2	14.7
SWD6	6.6	11.6	11.1
SWD8	18.1	18.9	14.2
SWD10	5.7	16.2	
SWD14	10	15.1	
SWD16	3.6	10	
SWD18	7.4	15.3	12.7
SWD20	10.5	13.3	12.9
SWD22	15.1	13.3	11.5
SWD23		48.7	
SWD24	11	16.2	10.4
SWD26	2.95	8.5	
SWD27	3.6	11.6	
SWD28	1.5	10	
SWD30A	10.2	20	
SWD30B	6.2	10.4	15.8
SWD31	5.2	12.2	
SWD32	8.5	15.8	13.6
SWD37	0.1	6.5	
SWD38	0.1	10	11.1
SWD39	7	14.7	10
SWD40	8.8	11.6	17.1
SWD41	6.2	13.5	8.5
SWD46	5.2	13.8	

Table B-4. Cone penetrometer depth profile data. (Depths are in inches.)

Site	Reading	Depth (in.)																		
		0	1	2	3	4	5	6	7	8	9.	10	11	12	13	14	15	16	17	18
SWD3	1		10	35	100	175	350	420												
	2			40	190	395	530	370	285	300	455	440	430	570						
	3		10	70	130	165	225	330	435	315	280	450								
	4	70	75	310	685	870														
SWD5	1	35	135	240	370	375	350	355	370	415	550									
	2	60	110	185	265	370	420	440	480	525	505	510	535	590						
	3	65	140	240	245	305	355	400	590											
SWD6	1			15	40	75	115	160	225	295	285	280	290	335	325	350				
	2			5	20	25	60	190	290	405	450									
	3	5	80	105	170	350	495	605	730											
	4	60	165	215	210	195	205	215	260	295	275	265	265	290	345	405				
	5	25	175	665	865	325	335	315	295	315	315	315	345	370	365	380	430			
	6	115	320	675	560	470	340	325	345	380	380	425	475	470	525	520	535			
SWD8	No data collected																			
SWD10	1		10	70	160	205	340	525												
	2		5	70	135	260	285	460	430	475										
	3		20	100	165	230	200	260	315	370	625	675	655	720						
	4	30	90	120	155	195	320	415	365	345	390	410	475							
	5	35	145	520																
	6	100	345																	
SWD14	1	120	180	300	470	510	755	795												
	2	25	170	345																
	3	70	95	300	440	600	875													
	4	25	95	235	300	430	555	695	585											
SWD16	1				15	95	175	260	320	360	460		435							
	2				25	105	195	305	325	185	215	425	535	610	530	520	540	220	295	315
	3			15	50	70	85	95	110	190	250	285	305	270	185	205	230	250	355	
SWD18	1	10	40	215	295	590	490	555	655	670	565	530								
	2	90	145	175	275	390	335	380	390	420	430	530	470	490						
	3	20	50	110	180	320	555	625	800											
SWD20	1			60	290	585	600													
	2		10	155	345	590														
	3	20	45	170	395	635														
	4	30	110	380	475															
	5		75	175	205	195	180	145	215	510										
	6	80	165	220	240	285	405	470	550	585	555	615	115							
	7	15	65	130	180	115	115	195	200	240	270	290	350	355	495					
SWD22	1	10	30	60	100	140	185	205	245	185	115	75	75	95	200	335	410			
	2	150	335	545	615	605	530	540	520	585	620	710	830							
	3	150	270	570	690	705	640	580	495	435	445	520	620							
SWD23	No data collected, surface too hard																			

Table B-4 (cont.). Cone penetrometer depth profile data. (Depths are in inches.)

Site	Reading	Depth (in.)																		
		0	1	2	3	4	5	6	7	8	9.	10	11	12	13	14	15	16	17	18
SWD24	1	50	80	130	230	430														
	2	10	50	155	270	430	670													
	3	20	50	245	430															
	4	15	35	165	670															
SWD26	1			20	30	50	65	95	155	285	370	440	540							
	2		10	40	60	100	275	420	655											
	3	5	25	80	130	180	230	270	330	475	615	690								
SWD27	1	5	35	60	75	85	100	120	130	130	145	160	175	205	230	275	295	270	260	270
	2	5	25	55	70	80	85	110	150	150	145	150	145	140	105	32	32	90	130	180
	3			35	55	65	80	90	115	145	185	205	170	185	195	190	165	65	30	55
	4		10	65	120	195	240	275	300	360	390	410								
	5			95	190	240	275	290	310	350	360	365	350	315	305	335	370	260	250	
	6		25	90	140	175	195	170	105	80	80	110	130							
	7	55	60	65	80	115	135	135	135	180	220	235								
	8	15	40	60	70	75	70	85	130	180	230	280	295	330	350	215		205		
SWD28	1				5	20	40	100	155	175	215	245								
	2				5	25	45	60	110	150	170	180	195	220	225	235	245	270	265	265
	3					10	25	60	75	80	90	100	100	95	105	105	115	115	115	135
	4			10	25	55	70	95	105	100	75	70	75	80	85	85	90	85		
	5		10	30	40	45	65	85	105	120	135	135	115	105	95	90	90	65	40	35
	6			10	30	55	80	100	135	145	150	140	120	110	85	55	40	35	35	30
SWD30A	1	55	115	250	315	420	410	545	530	630										
	2	65	200	405	415	580	610													
	3	50	195	225	250	260	260	265	250	290	320	310	340	430						
SWD30B	1		40	365	565	640	580	475	495	325	340	455	490							
	2	25	50	175	310	345	345	350	310	300	295	290	310	375	505					
	3		155	580	580	535	490	465	560	620										
SWD31	1	5	15	55	105	105	105	100												
	2	15	30	80	145	150	175	185												
	3	30	45	75	120	130	140													
	4		5	25	60	100	200	265	270	260	240	235	250	230	205	190	195	200	220	
	5		15	75	120	145	165	185	195	200	190	175	170	190						
SWD32	1	145	245																	
	2	195	350	585																
	3	175	240	435																
SWD37	1							15	80	100	105	115	170	415	485	480				
	2			20	20	15	25	70	90	130	145	480	530	495	480					
	3			20	30	25	15	5	40	80	110	295								
SWD38	1			25	45	70	100	140	175	195	195	200	190	190	180	130	120	110	85	95
	2	65	70	85	100	130	165	225	210	210	205	235	230	180	175	170	120	105		
	3	50	60	65	80	90	95	95	100	130	135	155	165	180	195	175	160	145	160	175

Table B-4 (cont.). Cone penetrometer depth profile data. (Depths are in inches.)

Site	Reading	Depth (in.)																		
		0	1	2	3	4	5	6	7	8	9.	10	11	12	13	14	15	16	17	18
SWD39	1		35	135	140	220	230	225	230	245	265	250	180	240	410	375	470			
	2	5	70	155	275	375	350	315	295	270	290	390	400	405	440	380	345	410	365	280
	3	15	140	265	320	290	355	435	475	535	510	495	465	510	520	525	505	475	430	430
SWD40	1	20	80	105	265	270	320			10										
	2	65	120	140	155	345	565	90	230	110	65	165	320	580	290	390				
	3	100	120	170	305	265	205	245	300	355	345	365	390							
	4	35	160																	
	5	45	70	640																
SWD41	1			45	145	230	270	280	305	290	265	230	215	260	325	375	455	480	465	460
	2	10	45	105	155	205	270	315												
	3	25	40	100	180	235	310	360	250	220	190	175	150							
	4			160	220	285	310	305	280	280	295	335	280	225	235	415	350			
SWD46	1		15	65	140	230	260	325	335	345	395	470	580	580	610	570	565	640		
	2		20	55	110	160	220	365	435	505	540	415								
	3	10	25	80	140	230	285	350	430	470	545	595	590	555	480	295	220			
PTD5A	average	120	336	814	917	720	738	881												
PTD5B	average	61	458	763	804	36														
PTD19	average	171	260	459	532	729	810	468												
PTD23A	average	302	456	587	535	531	490	514	520	560		611	629	687						
PTD23B	average	145	209	433	865	835	751	840												
PTD23C	average	51	214		881	814														
PTD23E	average	89	215	485	546	627	828	738												
PTD26B	average	54	70	145	202	349	473	239	840											
PTD29	average	63	158	378	672	829	877	879	765	797	942									
PTD32B	average	40	50	50	50	57	62	129	426	777										

Table B-5. Dynamic Cone Penetrometer data for SWD3 to SWD6.

SWD3-1 Light		SWD3-2 Light		SWD3-3 Heavy		SWD3-4 Heavy		SWD5-1 Heavy		SWD5-2 Heavy		SWD5-3 Heavy		SWD6-1 Heavy		SWD6-2 Heavy		SWD6-3 Heavy	
Blows	Depth (mm)	Blows	Depth (mm)	Blows	Depth (mm)	Blows	Depth (mm)	Blows	Depth (mm)	Blows	Depth (mm)	Blows	Depth (mm)	Blows	Depth (mm)	Blows	Depth (mm)	Blows	Depth (mm)
0	120	0	135	0	140	0	195	0	65	0	10	0	30	0	40	0	40	0	95
1	180	1	225	1	190	1	295	1	100	1	95	1	105	1	100	1	90	1	235
1	195	1	255	2	235	1	370	1	140	1	130	1	150	1	140	1	120	1	295
1	210	1	NA	2	280	1	405	1	165	1	185	1	195	1	175	1	150	1	335
1	220	1	660	2	330	1	420	1	185	1	230	1	240	1	210	1	180	1	365
1	230	1	680	2	380	1	435	1	205	1	260	1	275	1	240	1	205	1	390
1	240	1	685	2	425	1	450	1	230	1	285	1	305	1	270	1	235	1	410
1	245	3	700	2	465	1	460	1	250	1	305	1	320	1	300	1	260	1	430
1	250	3	720	2	500	1	475	1	275	1	330	1	345	1	325	1	285	1	445
1	260	3	735	2	535	1	490	1	290	1	350	1	365	1	335	1	310	1	460
1	265	3	740	2	565	1	505	2	310	1	370	1	395	1	375	1	335	1	470
1	270	5	760	2	595	1	525	4	325	1	390	1	425	1	400	1	360	1	480
1	280	5	775	2	620	1	545	4	335	1	410	1	450	1	420	1	380	1	500
1	285	5	790	2	640	1	565	8	360	1	430	1	470	1	440	1	410	1	510
1	290	5	810	2	660	1	585	1	370	1	450	1	495	1	465	1	430	1	525
1	295	5	830	2	680	1	605	1	380	1	465	1	500	1	490	1	450	1	545
1	300	5	840	2	695	1	620	1	395	1	480	1	525	1	515	1	461	1	570
1	310	5	855	2	715	1	630	1	410	1	500	1	570	1	540	1	480	1	600
1	312.5	5	865	2	730	1	640	1	420	1	520	1	590	1	560	1	505	1	630
1	320	10	885	2	745	1	650	1	435	1	540	1	605	1	580	1	520	1	660
1	322.5	10	905	2	760	1	660	1	445	1	550	1	625	1	600	1	530	1	690
1	330	10	925	2	780	2	680	1	460	1	560	1	545	1	620	1	550	1	715
1	340	10	945	2	790	2	690	1	475	1	580	1	570	1	640	1	560	1	745
1	350	10	965	3	810	2	705	1	490	1	590	1	590	1	655	1	575	1	770
1	355	5	980	3	830	2	720	1	505	1	610	1	605	1	670	1	590	1	790
1	360	5	980	3	855	2	740	1	520	1	630	1	625	1	680	1	600	1	810
1	367.5	5	990	3	875	2	755	1	535	1	645	1	645	1	690	1	615	1	835
1	370	5	1000	3	890	2	770	1	550	1	660	1	660	1	710	1	625	1	855
1	380			3	910	3	780	1	560	1	675	1	675	1	715	1	635	1	870
1	390			3	925	3	800	1	580	1	685	1	690	1	725	1	645	1	890
1	405			3	940	3	810	1	590	1	700	1	705	1	740	1	660		
1	420			3	950	3	825	1	605	1	715	1	720	1	750	1	670		
1	430			3	970	3	840	1	620	1	725	1	735	1	760	1	685		
1	450			3	990	3	855	2	645	1	735	1	750	1	770	1	695		
1	470			1	1000	3	870	1	665	1	750	1	765	1	770	1	710		
1	490					3	885	4	680	1	765	1	780	1	775	1	720		
1	510					3	900	8	725	1	780	1	795	1	790	1	730		
1	525					3	910	1	735	1	790	1	810	1	795	1	740		
1	540					3	920	1	745	1	800	1	825	1	800	1	750		
1	560					3	930	1	755	1	810	1	840	1	805	1	760		
1	575					3	940	1	765	1	825	1	855	1	810	1	770		
1	590							1	775	1	835	1	870	1	820	1	775		
1	600							1	785	1	850	1	885	1	830	1	785		
1	610							2	805	1	860			1	835	1	795		

Table B-5 (cont.). Dynamic Cone Penetrometer data for SWD3 to SWD6.

SWD3-1 Light		SWD3-2 Light		SWD3-3 Heavy		SWD3-4 Heavy		SWD5-1 Heavy		SWD5-2 Heavy		SWD5-3 Heavy		SWD6-1 Heavy		SWD6-2 Heavy		SWD6-3 Heavy	
Blows	Depth (mm)	Blows	Depth (mm)	Blows	Depth (mm)	Blows	Depth (mm)	Blows	Depth (mm)	Blows	Depth (mm)	Blows	Depth (mm)	Blows	Depth (mm)	Blows	Depth (mm)	Blows	Depth (mm)
1	625							2	830	1	870			1	840	1	800		
1	640							2	850	1	880			1	850	1	810		
1	650							1	870					1	855	1	815		
1	665													1	865	1	825		
1	680													1	875	1	830		
1	690													1	880	1	840		
1	700													1	890	1	845		
1	710															1	850		
1	720															1	860		
1	730															1	865		
1	740															1	875		
1	750															1	880		
1	760															1	890		
1	770																		
1	780																		
1	785																		
1	795																		
1	805																		
1	810																		
1	825																		
1	845																		
1	870																		
1	890																		
1	915																		
1	935																		
1	960																		
1	980																		
1	990																		
1	1000																		

Table B-6. Dynamic Cone Penetrometer data for SWD8 to SWD16.

SWD8-1 Heavy		SWD8-2 Heavy		SWD10-1 Light		SWD10-2 Heavy		SWD14-1 Heavy		SWD14-2 Heavy		SWD16-1 Light		SWD16-2 Light	
Blows	Depth (mm)	Blows	Depth (mm)	Blows	Depth (mm)	Blows	Depth (mm)	Blows	Depth (mm)	Blows	Depth (mm)	Blows	Depth (mm)	Blows	Depth (mm)
0	250	0	270	0	250	0	260	0	20	0	1	0	105	0	70
1	290	1	310	1	300	1	310	1	95	1	55	1	190	1	140
1	310	1	335	1	325	1	325	1	120	1	80	1	230	1	170
1	330	1	365	1	340	1	340	1	145	1	100	1	260	1	195
1	345	1	405	1	360	1	355	1	170	1	110	1	280	1	215
1	365	1	450	1	370	1	370	1	190	1	120	1	290	1	230
1	380	1	490	1	380	1	380	1	200	1	135	1	305	1	250
1	395	1	515	1	390	1	390	1	210	1	145	1	315	1	275
1	420	1	535	1	395	1	410	1	220	1	155	1	325	1	300
1	445	1	550	1	400	1	420	1	230	1	165	1	335	1	315
1	470	1	560	1	405	1	440	1	240	1	170	1	345	1	325
1	510	1	570	4	420	1	450	1	245	1	180	1	360	1	335
1	540	1	580	4	440	1	460	1	255	1	190	1	370	1	350
1	580	1	590	4	460	1	475	1	270	1	205	1	380	1	360
1	590	1	595	4	480	1	485	1	290	1	215	1	395	1	375
1	605	1	600	4	495	1	495	1	310	1	225	1	410	1	390
1	620	3	620	6	510	1	505	1	335	1	240	1	430	1	400
1	625	3	640	6	530	1	515	1	350	1	255	1	450	1	410
1	630	3	660	6	550	1	520	1	365	1	265	1	470	1	420
1	640	3	690	6	570	1	530	1	380	1	275	1	485	1	430
1	645	3	720	6	600	1	540	1	390	1	295	1	510	1	440
3	660	3	740	6	625	1	545	1	405	1	305	1	530	1	450
3	680	3	760	6	650	1	550	1	425	1	325	1	550	1	455
3	690	3	775	6	670	3	570	1	440	1	350	1	570	1	465
3	710	3	790	6	685	3	590	1	455	1	390	1	595	1	480
3	730	3	805	6	710	3	610	1	470	1	420	1	610	1	485
3	750	3	815	6	730	3	640	1	490	1	475	1	630	1	490
3	765	3	825	6	760	3	670	1	510	1	535	1	640	1	495
3	780	3	835	6	780	3	700	1	525	1	595	1	655	1	500
3	810	3	840	6	810	3	740	1	535	1	605	1	665	3	520
3	820	3	855	6	845	3	775	1	545	1	610	1	680	3	540
3	830	3	870	6	880	3	810	1	560	1	650	1	695	3	565
3	845	3	880	6	900	3	840	1	575	1	670	1	705	3	580
3	860	3	890	6	930	3	870	1	585	1	680	1	725	3	600
3	870	3	905	6	955	3	890	1	595	1	700	1	735	3	620
3	880	3	920	6	980	3	905	1	610	1	710	1	750	3	640

Table B-6 (cont.). Dynamic Cone Penetrometer data for SWD8 to SWD16.

SWD8-1 Heavy		SWD8-2 Heavy		SWD10-1 Light		SWD10-2 Heavy		SWD14-1 Heavy		SWD14-2 Heavy		SWD16-1 Light		SWD16-2 Light	
Blows	Depth (mm)	Blows	Depth (mm)	Blows	Depth (mm)	Blows	Depth (mm)	Blows	Depth (mm)	Blows	Depth (mm)	Blows	Depth (mm)	Blows	Depth (mm)
3	895	3	930	3	1000	3	915	1	620	1	730	1	760	3	655
3	910	3	945			3	930	1	640	1	750			3	680
3	920	3	965			3	940	1	660					3	700
3	935	3	980			3	945	1	685					3	720
3	950	3	1000			3	955	1	700					3	740
3	970					3	960	1	715					3	755
3	990					3	970	1	740					1	760
1	1000					3	980								
						3	985								
						3	990								
						3	995								
						3	1000								

Table B-7. Dynamic Cone Penetrometer data for SWD22 to SWD26.

SWD22-1 Heavy		SWD22-2 Heavy		SWD22-3 Heavy		SWD23-1 Heavy		SWD24-1 Heavy		SWD24-2 Heavy		SWD26-1 Light		SWD26-2 Light	
Blows	Depth (mm)	Blows	Depth (mm)	Blows	Depth (mm)	Blows	Depth (mm)	Blows	Depth (mm)	Blows	Depth (mm)	Blows	Depth (mm)	Blows	Depth (mm)
0	70	0	5	0	130	0	250	0	260	0	40	0	25	0	45
1	105	1	60	1	210	1	275	1	340	1	100	1	110	1	130
1	130	1	90	1	300	1	290	1	360	1	120	1	155	1	180
1	155	1	130	1	355	1	295	1	380	1	135	1	190	1	210
1	180	1	165	1	400	1	300	1	390	1	150	1	215	1	235
1	200	1	190	1	435	4	330	1	400	1	160	1	240	1	260
1	215	1	210	1	455	4	350	1	420	1	175	1	260	1	280
1	230	1	235	1	475	4	370	1	430	1	190	1	275	1	310
1	250	1	255	1	490	4	385	1	440	1	200	1	290	1	340
1	265	1	280	1	510	4	390	1	450	1	220	1	305	1	360
1	285	1	300	1	530	6	400	1	460	1	235	1	315	1	385
1	310	1	320	1	550	6	410	1	470	1	250	1	325	1	410
1	340	1	335	1	580	6	415	1	480	1	265	1	345	1	425
1	370	1	360	1	605	6	415	1	490	1	280	1	355	1	440
1	390	1	375	1	630	10	420	1	500	1	300	1	365	1	455
1	410	1	390	1	650	10	425	1	515	1	320	1	380	1	470
1	420	1	400	1	670	10	430	1	525	1	335	1	385	1	480
1	440	1	410	1	685	10	440	1	540	1	350	1	405	1	500
1	450	1	420	1	700	10	440	1	550	1	370	1	425	1	510
1	460	1	430	1	710	10	440	1	565	1	390	1	435	1	525
1	470	1	440	1	725			1	580	1	410	1	445	1	540
1	480	1	445	1	740			1	590	1	430	1	460	1	555
1	495	1	460	1	750			1	600	1	450	1	475	1	565
1	505	1	460					1	615	1	470	1	485	1	580
1	510	1	470					1	630	1	490	1	495	1	600
1	520	1	480					1	640	1	510	1	505	1	610
1	535	1	490					1	660	1	525	1	515	1	625
1	545	1	500					1	670	1	545	1	525	1	630
1	560	1	510					1	690	1	560	1	535	1	640
1	570	1	520					1	705	1	580	1	550	1	650
1	580	1	530					1	720	1	600	1	560	1	660
1	595	1	540					1	735	1	620	1	570	1	670
1	605	1	555					1	750	1	640	1	585	1	675
1	615	1	570					1	770	1	670	1	595	1	690
1	625	1	580					1	785	1	690	1	610	1	700
1	630	1	585					1	800	1	710	1	625	1	705

Table B-7 (cont.). Dynamic Cone Penetrometer data for SWD22 to SWD26.

SWD22-1 Heavy		SWD22-2 Heavy		SWD22-3 Heavy		SWD23-1 Heavy		SWD24-1 Heavy		SWD24-2 Heavy		SWD26-1 Light		SWD26-2 Light	
Blows	Depth (mm)	Blows	Depth (mm)	Blows	Depth (mm)	Blows	Depth (mm)	Blows	Depth (mm)	Blows	Depth (mm)	Blows	Depth (mm)	Blows	Depth (mm)
1	640	1	600					1	815	1	730	1	635	1	715
1	650	1	610					1	830	1	750	1	650	1	720
1	655	1	625					1	840			1	665	1	730
1	660	1	640					1	855			1	680	1	740
1	670	1	650					1	870			1	695	1	750
1	680	1	660					1	880			1	710	1	760
1	685	1	675					1	895			1	725		
1	700	1	685					1	910			1	745		
1	705	1	690					1	920						
1	710	1	700					1	930						
1	720	1	705					1	940						
1	725	1	710					1	955						
1	730	1	720					1	970						
1	740	1	730					1	980						
1	745	1	735					1	990						
1	750	1	740					1	1000						
1	755	1	747												
1	760	1	755												
1	765	1	760												
1	770	2	775												
1	775	2	780												
1	780	2	800												
1	780	2	810												
1	785	2	820												
1	790	2	830												
1	800	2	845												
1	805	2	860												
2	805	2	875												
4	810	1	885												
5	830	1	892												
5	845														
5	850														
5	870														
5	880														
5	885														
5	900														

Table B-8. Dynamic Cone Penetrometer data for SWD27 to SWD28.

SWD27-1 Light		SWD27-2 Light		SWD27-3 Light		SWD27-4 Light		SWD28-1 Light		SWD28-2 Light		SWD28-3 Light		SWD28-4 Light	
Blows	Depth (mm)	Blows	Depth (mm)	Blows	Depth (mm)	Blows	Depth (mm)	Blows	Depth (mm)	Blows	Depth (mm)	Blows	Depth (mm)	Blows	Depth (mm)
0	30	0	40	0	35	0	25	0	100	0	60	0	55	0	50
1	155	1	160	1	115	1	100	1	180	1	200	1	170	1	155
1	250	1	230	1	150	1	165	1	230	1	540	1	240	1	210
1	300	1	290	1	180	1	210	1	290	1	780	1	290	1	250
1	325	1	335	1	200	1	235	1	400			1	340	1	300
1	355	1	375	1	235	1	260	1	470			1	380	1	370
1	380	1	410	1	260	1	280	1	520			1	480	1	580
1	415	1	445	1	305	1	300	1	565			1	770	1	810
1	455	1	490	1	360	1	315	1	615						
1	510	1	530	1	400	1	335	1	745						
1	590	1	575	1	430	1	350								
1	690	1	600	1	470	1	365								
1	760	1	625	1	500	1	380								
		1	650	1	560	1	400								
		1	670	1	615	1	415								
		1	695	1	640	1	430								
		1	715	1	655	1	445								
		1	730	1	675	1	460								
		1	745	1	690	1	470								
		1	760	1	710	1	485								
				1	730	1	500								
				1	750	1	515								
						1	525								
						1	540								
						1	560								
						1	580								
						1	600								
						1	620								
						1	645								
						1	690								
						1	770								

Table B-9. Dynamic Cone Penetrometer data for SWD30A to SWD32.

SWD30A-1 Light		SWD30A-2 Heavy		SWD30B-1 Heavy		SWD30B-2 Heavy		SWD31-1 Light		SWD31-2 Light		SWD32-1 Heavy		SWD32-2 Heavy	
Blows	Depth (mm)	Blows	Depth (mm)	Blows	Depth (mm)	Blows	Depth (mm)	Blows	Depth (mm)	Blows	Depth (mm)	Blows	Depth (mm)	Blows	Depth (mm)
0	275	0	15	0	50	0	40	0	45	0	50	0	10	0	80
1	340	1	105	1	145	1	125	1	120	1	150	1	50	1	105
1	365	1	155	1	220	1	165	1	165	1	200	1	70	1	120
1	390	1	195	1	265	1	195	1	205	1	235	1	85	1	130
1	410	1	230	1	290	1	225	1	245	1	265	1	95	1	140
1	430	1	255	1	300	1	245	1	285	1	290	1	110	1	150
1	440	1	275	1	315	1	270	1	325	1	335	1	120	1	155
1	450	1	295	1	330	1	285	1	360	1	370	1	130	1	160
1	460	1	320	1	340	1	295	1	390	1	405	1	130	4	180
1	470	1	340	1	350	1	300	1	425	1	440	1	135	4	195
1	480	1	357.5	1	360	1	310	1	460	1	470	1	145	8	220
1	490	1	370	1	370	1	320	1	485	1	505	1	155	8	240
1	497.5	1	375	1	375	1	325	1	505	1	535	1	160	8	265
1	505	1	385	1	380	1	335	1	530	1	565	2	180	8	290
1	510	1	392.5	1	385	1	340	1	555	1	595	2	200	8	305
1	520	3	402.5	3	400	3	345	1	580	3	615	2	215	10	345
1	530	3	415	3	420	3	350	1	600	3	635	2	230	10	365
1	535	3	425	3	440	3	360	1	625	3	655	2	240	10	390
1	540	3	435	3	460	3	370	1	645	3	675	2	255	10	410
1	550	3	445	3	470	3	380	1	665	3	685	2	260	10	425
1	557.5	3	450	3	485	3	390	1	685	3	705	4	275	10	450
1	565	3	460	3	500	3	395	1	710	3	725	4	295	20	450
1	570	3	475	3	515	3	400	1	735	3	735	4	305		
1	580	3	485	3	520	5	405	1	765	5	745	4	320		
1	585	3	495	3	530	5	405					4	330		
1	590	3	505	3	540	10	410					4	350		
3	610	3	515	3	550	10	412					4	360		
3	620	3	520	3	555							4	380		
3	635	3	532.5	6	570							5	400		
3	645	3	535	6	590							5	420		
3	655	3	545	6	600							5	440		
3	670	3	555	6	620							5	455		
3	675	3	560	6	635							5	475		
3	685	3	600	6	645							5	490		
3	695	3	615	8	650							5	510		
5	700	3	625	10	660							5	530		

Table B-9 (cont.). Dynamic Cone Penetrometer data for SWD30A to SWD32.

SWD30A-1 Light		SWD30A-2 Heavy		SWD30B-1 Heavy		SWD30B-2 Heavy		SWD31-1 Light		SWD31-2 Light		SWD32-1 Heavy		SWD32-2 Heavy	
Blows	Depth (mm)	Blows	Depth (mm)	Blows	Depth (mm)	Blows	Depth (mm)	Blows	Depth (mm)	Blows	Depth (mm)	Blows	Depth (mm)	Blows	Depth (mm)
5	715	3	635	10	675							5	540		
5	730	3	655	10	685							5	560		
5	745	3	665	15	690							5	570		
5	760	3	670	20	690							5	585		
5	770	3	680	20	690							5	595		
5	780	3	685									5	610		
5	790	3	690									5	625		
5	795	3	695									5	635		
8	805	3	705									4	650		
8	815	3	715									5	660		
8	820	3	730									5	665		
8	825	3	740									5	670		
10	830	2	745									10	670		
10	830											20	670		
10	840														
10	840														
10	840														
20	847.5														
20	860														
20	860														

Table B-10. Dynamic Cone Penetrometer data for SWD37 to SWD39.

SWD37-1 Light		SWD37-2 Light		SWD38-1 Light		SWD38-2 Light		SWD39-1 Light		SWD39-2 Light	
Blows	Depth (mm)	Blows	Depth (mm)	Blows	Depth (mm)	Blows	Depth (mm)	Blows	Depth (mm)	Blows	Depth (mm)
0	180	0	105	0	70	0	250	0	260	0	265
1	250	1	160	1	210	1	380	1	340	1	325
1	280	1	200	1	275	1	440	1	360	1	360
1	310	1	230	1	335	1	490	1	380	1	380
1	330	1	265	1	405	1	540	1	390	1	395
1	360	1	300	1	465	1	635	1	400	1	405
1	390	1	330	1	530	1	770	1	415	1	420
1	420	1	355	1	575	1	805	1	430	1	430
1	450	1	380	1	610	1	860	1	440	1	440
1	475	1	400	1	645	1	900	1	445	1	450
1	500	1	420	1	680	1	925	2	465	1	457.5
1	520	1	440	1	725	1	955	2	480	1	467.5
1	540	1	460	1	815	1	1000	2	505	1	480
1	570	1	480					2	525	1	485
1	600	1	505					2	550	1	500
1	620	1	530					2	570	1	510
1	640	1	550					2	590	1	520
1	655	1	570					2	620	1	525
1	680	1	585					2	650	1	540
1	695	1	600					2	670	1	550
1	720	1	620					2	695	1	570
1	740	1	640					2	720	1	575
1	760	1	660					2	745	2	600
		1	680					2	770	2	622.5
		1	700					2	795	2	650
		1	720					2	820	2	670
		1	740					2	850	2	695
		1	755					2	880	2	720
								2	905	2	745
								2	940	2	770
								2	970	2	800
								2	1005	2	825
										2	850
										2	880
										2	895
										2	930
										2	960
										1	1005

Table B-11. Dynamic Cone Penetrometer data for SWD40 to SWD46.

SWD40-1 Heavy		SWD40-2 Heavy		SWD41-1 Heavy		SWD41-2 Heavy		SWD46-1 Light		SWD46-2 Light	
Blows	Depth (mm)	Blows	Depth (mm)	Blows	Depth (mm)	Blows	Depth (mm)	Blows	Depth (mm)	Blows	Depth (mm)
0	5	0	15	0	55	0	15	0	40	0	35
1	115	1	35	1	145	1	100	1	110	1	105
1	175	1	50	1	190	1	155	1	145	1	175
1	205	1	55	1	235	1	205	1	180	1	205
1	240	1	65	1	275	1	260	1	210	1	220
1	280	1	75	1	310	1	345	1	240	1	230
1	310	1	85	1	345	1	440	1	260	1	260
1	350	1	95	1	375	1	480	1	290	1	275
1	380	1	105	1	405	1	505	1	300	1	290
1	550	2	125	2	430	2	530	1	320	1	300
1	570	2	150	2	455	2	560	1	330	1	310
1	595	2	175	2	475	2	580	1	350	1	320
1	615	2	200	2	495	2	595	1	360	1	330
1	640	2	220	2	510	2	610	1	375	1	345
1	680	2	235	2	535	2	625	1	390	1	355
1	710	2	255	2	545	2	640	1	400	1	365
1	730	2	275	2	565	2	655	1	415	1	370
1	740	2	305	2	585	2	665	1	430	1	390
1	750	2	340	2	605	2	675	1	440	1	400
		2	375	2	615	2	690	1	455	1	405
		1	395	1	635	1	700	1	470	1	425
		1	415	1	645	1	710	1	480	1	435
		1	435	1	655	1	720	1	490	1	445
		1	455	1	680	1	730	1	505	1	455
		1	475	1	690	1	740	1	520	1	470
		1	495	1	695			1	530	1	475
		1	505	1	707.5			1	540	1	485
		1	525	1	735			1	550	1	500
		1	545	1	745			1	565	1	510
		1	555	1	775			1	575	1	520
		1	570					1	590	1	535
		1	580					1	595	1	545
		1	595					1	610	1	555
		1	605					1	620	1	570
		1	620					1	630	1	585
		1	630					1	640	1	595

Table B-11 (cont.). Dynamic Cone Penetrometer data for SWD40 to SWD46.

SWD40-1 Heavy		SWD40-2 Heavy		SWD41-1 Heavy		SWD41-2 Heavy		SWD46-1 Light		SWD46-2 Light	
Blows	Depth (mm)	Blows	Depth (mm)	Blows	Depth (mm)	Blows	Depth (mm)	Blows	Depth (mm)	Blows	Depth (mm)
		1	645					1	650	1	605
		1	655					1	660	1	617.5
		1	665					1	675	1	630
		1	675					1	690	1	642.5
		1	685					1	715	1	655
		1	695					1	725	1	665
		1	705					1	740	1	675
		1	715					1	750	1	685
		1	725							1	695
		1	735							1	705
		1	745							1	715
										1	725
										1	735
										1	745

Table B-12. Dynamic Cone Penetrometer data for PTD5A to PTD21B.

PTD5A-1 Heavy		PTD5B-1 Heavy		PTD8A-1 Heavy		PTD8B-1 Heavy		PTD19-1 Heavy		PTD21A-1 Heavy		PTD21B-1 Heavy	
Blows	Depth (mm)	Blows	Depth (mm)	Blows	Depth (mm)	Blows	Depth (mm)	Blows	Depth (mm)	Blows	Depth (mm)	Blows	Depth (mm)
0	65	0	50	0	80	0	60	0	70	0	45	0	50
1	105	1	90	1	100	1	75	1	140	1	75	1	100
1	135	1	110	1	115	1	90	1	175	1	95	1	130
1	160	1	135	1	130	1	100	1	205	1	105	1	145
1	175	1	160	1	150	2	125	1	230	1	115	1	160
1	190	1	180	1	170	2	160	1	250	2	135	1	170
1	200	1	200	1	200	2	190	1	265	2	150	1	180
2	230	1	230	1	230	2	220	1	285	2	170	2	200
1	245	1	245	1	250	2	250	1	310	2	185	2	210
1	260	1	260	1	270	2	275	1	330	2	210	2	220
1	270	1	270	1	290	2	300	1	350	2	245	4	245
1	280	1	285	1	305	2	320	1	360	1	270	4	265
2	300	1	300	1	320	2	335	1	375	1	295	4	280
2	315	1	310	1	335	2	345	2	410	1	325	4	290
2	325	1	320	1	350	2	360	2	440	1	355	5	305
2	335	1	335	1	370	2	375	2	480	1	385	7	330
2	345	1	350	1	380	2	385	2	520	1	420	7	345
4	365	2	370	1	395	4	410	2	550	1	445	7	360
4	380	2	390	2	420	4	430	2	590	1	475	10	380
4	390	2	405	2	450	4	445	2	610	1	505	10	395
6	405	2	420	2	480	4	460	2	640	1	540	15	415
6	420	2	440	2	490	6	480	2	670	1	570	15	420
6	435	2	455	2	510	6	500	2	700	1	595	20	420
10	460	3	480	2	530	6	520	2	720	1	620	20	420
10	480	3	510	2	545	6	540	2	740	1	645		
20	520	3	535	2	560	6	555	2	765	1	675		
20	550	3	560	2	580	6	570	2	790	1	720		
20	590	3	585	2	590	8	595	2	810	1	785		
20	620	3	610	4	620	8	610	2	830	1	910		
20	660	3	640	3	635	10	635	2	850	1	960		
20	720	3	665	3	650	10	665	2	870	1	1000		
15	760	3	690	4	670	10	690	2	890				
10	780	3	710	4	690	10	720	2	915				
10	810	3	735	4	705	10	750	2	930				
10	840	3	755	4	720	10	785	2	955				
10	865	3	780	4	735	10	820	2	975				

Table B-12 (cont.). Dynamic Cone Penetrometer data for PTD5A to PTD21B.

PTD5A-1 Heavy		PTD5B-1 Heavy		PTD8A-1 Heavy		PTD8B-1 Heavy		PTD19-1 Heavy		PTD21A-1 Heavy		PTD21B-1 Heavy	
Blows	Depth (mm)	Blows	Depth (mm)	Blows	Depth (mm)	Blows	Depth (mm)	Blows	Depth (mm)	Blows	Depth (mm)	Blows	Depth (mm)
10	900	3	800	4	750	10	865	2	995				
10	930	3	825	4	770	10	895	1	1000				
10	960	3	840	4	790	10	920						
10	985	3	860	4	810	10	940						
		3	880	4	830	10	955						
		3	900	4	850	10	985						
		3	915	4	870	5	1000						
		3	930	4	890								
		3	950	4	915								
		3	965	4	935								
		3	980	4	955								
		3	1000	4	975								
				4	995								
				2	1000								

Table B-13. Dynamic Cone Penetrometer data for PTD22 to PTD23E.

PTD22-1 Heavy		PTD23A-1 Heavy		PTD23B-1 Heavy		PTD23B-2 Heavy		PTD23C-1 Heavy		PTD23D-1 Heavy		PTD23E-1 Heavy	
Blows	Depth (mm)	Blows	Depth (mm)	Blows	Depth (mm)	Blows	Depth (mm)	Blows	Depth (mm)	Blows	Depth (mm)	Blows	Depth (mm)
0	60	0	65	0	115	0	65	0	70	0	60	0	60
1	90	1	120	1	265	1	130	1	105	1	100	1	125
1	105	1	170	1	390	1	180	1	120	1	125	1	160
1	120	1	240	1	485	1	240	1	140	1	145	1	185
1	140	1	305	1	560	1	290	1	160	1	170	1	200
2	155	1	360	1	650	1	335	1	170	1	190	1	210
2	170	1	420	1	680	1	390	1	185	1	220	1	220
2	185	1	465	1	690	1	430	1	200	1	250	2	240
2	200	1	510	1	695	1	495	1	220	1	280	2	255
2	215	1	545	2	710	1	555	1	235	1	320	2	270
2	230	1	560	2	730	1	610	1	250	1	365	3	290
1	245	1	570	2	745	1	650	1	260	1	410	3	315
1	260	2	580	2	770	1	690	2	280	1	465	3	330
1	270	4	600	2	800	1	730	2	305	1	540	4	360
1	285	4	615	2	845	1	765	2	330	1	610	4	385
1	290	4	630	2	945	1	805	2	360	1	670	4	410
1	305	6	660	1	1000	1	860	2	390	1	730	4	445
2	325	6	700			1	1000	2	435	1	780	4	480
2	345	4	740					1	460	1	840	4	515
2	355	4	775					1	490	1	890	4	560
2	370	4	830					1	515	1	930	4	610
2	380	2	850					1	530	1	965	4	670
2	390	2	870					1	540	1	985	2	700
4	410	2	885					2	560	1	1010	2	725
4	435	2	900					2	570			2	745
4	450	2	925					4	590			2	780
4	470	2	950					4	620			2	800
4	485	2	980					4	665			2	820
4	500	2	990					2	690			2	840
4	515							2	745			2	860
6	540							1	780			2	875
6	565							1	830			2	895
6	595							1	880			2	910
6	620							1	920			2	930
6	645							1	955			2	945
6	670							1	990			2	960

Table B-13 (cont.). Dynamic Cone Penetrometer data for PTD22 to PTD23E.

PTD22-1 Heavy		PTD23A-1 Heavy		PTD23B-1 Heavy		PTD23B-2 Heavy		PTD23C-1 Heavy		PTD23D-1 Heavy		PTD23E-1 Heavy	
Blows	Depth (mm)	Blows	Depth (mm)	Blows	Depth (mm)	Blows	Depth (mm)	Blows	Depth (mm)	Blows	Depth (mm)	Blows	Depth (mm)
6	695											2	975
6	715											2	985
6	740											2	995
6	765											1	100
6	785												
6	810												
6	840												
6	870												
4	890												
4	910												
4	930												
4	950												
4	965												
4	985												
4	1000												

Table B-14. Dynamic Cone Penetrometer data for PTD25A to PTD26A.

PTD25A-1 Light		PTD25A-2 Heavy		PTD25B-1 Heavy		PTD25C-1 Heavy		PTD26A-1 Heavy		PTD26A-2 Light	
Blows	Depth (mm)	Blows	Depth (mm)	Blows	Depth (mm)	Blows	Depth (mm)	Blows	Depth (mm)	Blows	Depth (mm)
0	55	0	60	0	65	0	55	0	60	0	55
1	80	1	125	1	120	1	90	1	115	1	75
1	90	1	160	1	150	1	110	1	150	1	90
1	105	1	180	1	160	1	130	1	195	1	100
1	115	1	205	1	170	1	145	1	245	1	110
2	135	1	225	1	180	1	150	1	290	1	125
2	155	1	240	1	195	1	160	1	325	1	140
2	180	1	250	1	210	1	170	1	400	1	160
2	200	1	265	1	225	1	180	1	445	1	185
2	220	1	275	1	240	1	195	1	470	1	210
2	240	1	285	1	250	1	210	1	490	1	235
2	255	1	290	1	265	1	220	1	505	1	255
2	265	2	310	1	285	1	235	1	520	1	280
2	275	2	330	1	300	1	245	1	535	1	300
3	285	2	350	1	320	1	260	1	555	1	320
3	300	2	360	1	335	1	265	1	570	1	335
3	310	2	380	1	350	2	285	1	580	1	350
4	330	2	390	1	360	2	300	1	595	1	360
4	355	2	400	1	370	2	320	1	610	1	380
4	370	2	410	1	380	2	340	1	625	1	385
4	395	2	420	1	395	2	360	1	640	1	395
4	415	2	430	1	400	2	370	1	650	2	415
4	435	2	440	1	420	3	390	1	660	2	440
4	450	2	445	1	430	3	405	1	670	2	460
4	460	3	460	1	440	5	425	1	680	2	480
4	475	3	470	1	445	5	435	1	690	2	500
4	490	4	480	1	455	5	445	1	700	2	520
4	500	4	505	2	475	5	455	1	710	2	540
4	515	4	515	2	490	5	465	2	735	2	560
5	530	4	535	2	505	5	475	2	760	2	580
5	540	4	550	2	520	10	500	2	785	2	600
5	545	4	565	2	535	10	525	2	810	2	620
5	560	4	580	2	550	10	550	2	830	2	645
5	570	4	590	3	570	10	580	2	860	2	670
5	580	5	610	3	590	10	605	2	880	2	695
5	585	5	630	3	615	10	625	2	910	2	710

Table B-14 (cont.). Dynamic Cone Penetrometer data for PTD25A to PTD26A.

PTD25A-1 Light		PTD25A-2 Heavy		PTD25B-1 Heavy		PTD25C-1 Heavy		PTD26A-1 Heavy		PTD26A-2 Light	
Blows	Depth (mm)	Blows	Depth (mm)	Blows	Depth (mm)	Blows	Depth (mm)	Blows	Depth (mm)	Blows	Depth (mm)
5	600	5	650	3	635	10	650	2	935	2	730
		5	665	3	655	10	675	2	965	2	750
		5	685	3	670	10	695	2	990	2	760
		5	700	3	680	10	715	1	1010	2	775
		5	720	3	700	10	740			3	790
		5	750	3	710	10	775			3	810
		5	770	3	730	10	795			3	820
		5	790	3	745	10	810			3	845
		5	810	3	760	10	830			3	865
		5	830	3	770	10	850			3	880
		5	850	4	790	10	860			3	890
		5	870	4	810	10	880			3	905
		5	890	4	825	10	895			3	910
		5	920	3	830	10	915			4	925
		5	940	3	840	10	940			4	935
		5	960	4	855	10	955			5	955
		5	990	4	870	10	970			5	965
		2	1000	4	895					5	980
				4	910					5	990
				4	925					5	1000
				4	940						
				4	955						
				4	970						
				3	980						
				3	990						
				2	1000						

Table B-15. Dynamic Cone Penetrometer data for PTD29 to PTD34.

PTD29-1 Heavy		PTD32A-1 Heavy		PTD32B-1 Light		PTD34-1 Heavy	
Blows	Depth (mm)	Blows	Depth (mm)	Blows	Depth (mm)	Blows	Depth (mm)
0	70	0	50	0	230	0	60
1	135	1	90	1	250	1	100
1	200	1	115	1	260	1	115
1	235	1	135	1	265	1	130
1	255	1	150	1	275	1	140
1	270	1	170	1	280	1	150
1	280	1	190	1	285	1	160
1	295	1	210	2	295	1	170
1	305	2	220	2	300	1	175
1	315	2	240	2	310	2	190
1	330	2	260	2	315	2	210
1	340	2	270	3	330	2	225
1	350	3	285	3	340	2	245
2	380	3	300	3	355	2	265
2	410	3	310	4	370	2	285
2	440	4	325	4	380	2	300
2	490	4	340	4	390	2	315
2	525	4	355	4	410	2	330
2	560	4	370	4	425	2	345
2	600	4	385	4	440	2	360
2	620	4	400	4	455	2	375
2	650	4	415	4	475	2	390
2	680	4	430	4	480	2	400
2	710	4	440	4	495	2	415
2	735	4	455	5	520	3	430
2	765	5	470	5	535	3	450
2	790	5	480	5	570	3	465
2	820	5	495	5	590	3	480
2	855	5	510	5	600	4	490
2	880	5	520	5	610	4	510
2	920	5	540	7	620	4	520
2	955	7	550	7	640	3	530
2	1000	7	560	7	670	4	550
		7	570	10	690	4	560
		2	590	10	700	5	580
		2	615	10	710	5	595
		2	650	15	730	7	620

Table B-15 (cont.). Dynamic Cone Penetrometer data for PTD29 to PTD34.

PTD29-1 Heavy		PTD32A-1 Heavy		PTD32B-1 Light		PTD34-1 Heavy	
Blows	Depth (mm)	Blows	Depth (mm)	Blows	Depth (mm)	Blows	Depth (mm)
		2	675	15	750	7	635
		2	695	15	780	10	655
		2	710	15	820	10	670
		2	740	15	870	12	695
		2	750	15	930	12	730
		2	770	5	960	12	770
		1	780	5	985	10	810
		2	790	4	1000	10	855
		2	800			10	900
		2	820			10	945
		2	825			10	980
		2	830			8	1000
		4	850				
		4	865				
		4	880				
		4	900				
		4	920				
		4	935				
		4	960				
		4	980				
		4	1000				

Table B-16. Average surface soil USDA texture.

Site	USDA Class	USCS Class	<2 mm Volume (%)		
			Clay	Silt	Sand
SWD3	Fine Sand	SP-SM	4	3	93
SWD5	Fine Sand	SM	0	8	92
SWD6	Fine Sand	SP-SM	0	5	95
SWD8	Sandy Loam	SM	5	27	68
SWD10	Fine Sand	SW/SP	1	5	94
SWD14	Silt Loam	ML-CL	7	73	20
SWD16	Fine Sand	SW/SP	1	5	94
SWD18	Silt Loam	SM	3	56	41
SWD20	Sandy Loam	SP-SM	5	35	59
SWD22	Silt Loam	SM-SC/SC	10	53	37
SWD23	Sandy Loam	SM	7	31	62
SWD24	Loamy Fine Sand	SM	3	19	78
SWD26	Fine Sand	SW/SP	1	1	98
SWD27	Fine Sand	SW/SP	0	2	98
SWD28	Fine Sand	SW/SP	0	2	98
SWD30A	Loamy Fine Sand	SM	2	17	81
SWD30B	Fine Sand	SM	1	12	86
SWD31	Fine Sand	SW/SP	0	3	97
SWD32	Sandy Loam	ML	6	43	51
SWD37	Fine Sand	SW/SP	0	5	95
SWD38	Sandy Loam	SM	2	37	62
SWD39	Silt Loam	ML-CL	4	68	28
SWD40	Sandy Loam	SM	2	33	65
SWD41	Fine Sand	SP-SM/SM	1	6	93
SWD46	Fine Sand	SW/SP	0	2	98
PTD5A	Silt	ML	6	80	14
PTD5B	Silt Loam	ML	10	73	17
PTD8A	Silt Loam	ML	11	61	28
PTD8B	Sandy Loam	CL	17	30	53
PTD19	Silt Loam	ML-CL	10	72	18
PTD21A	Sandy Loam	SM	7	26	67
PTD21B	Silt Loam	CL	18	51	31
PTD22	Silt Loam	ML-CL	8	63	29
PTD23A	Silt Loam	ML-CL	9	56	35
PTD23B	Loam	ML	8	40	52
PTD23C	Silt Loam	CL	14	68	17
PTD23D	Silt Loam	ML-CL	11	73	16
PTD23E	Silt Loam	ML	7	59	34

Table B-16 (cont.). Average surface soil USDA texture.

Site	USDA Class	USCS Class	<2 mm Volume (%)		
			Clay	Silt	Sand
PTD25A	Sandy Loam	SM	4	22	74
PTD25B	Sandy Loam	SM	2	36	61
PTD25C	Sandy Loam	ML	3	44	53
PTD26A	Sandy Loam	ML	3	44	54
PTD26B	Sandy Loam	ML	3	43	54
PTD29	Sandy Loam	SM	3	35	62
PTD32A	Silt Loam	ML	4	59	38
PTD32B	Silt Loam	ML	8	71	21
PTD34	Silt Loam	ML	6	58	36

REPORT DOCUMENTATION PAGE

Form Approved
OMB No. 0704-0188

1. REPORT DATE *(DD-MM-YYYY)*	**2. REPORT TYPE**	**3. DATES COVERED** *(From - To)*
August 2018	Technical Report/Final	

4. TITLE AND SUBTITLE

Soil Strength Analysis of Sonoran Desert Landforms

5a. CONTRACT NUMBER

5b. GRANT NUMBER

5c. PROGRAM ELEMENT NUMBER
T42 P2 448312 and 5L923J

6. AUTHOR(S)

Sally A. Shoop, Samuel A. Beal, Wendy L. Wieder, and Eric V. McDonald

5d. PROJECT NUMBER

5e. TASK NUMBER

5f. WORK UNIT NUMBER

7. PERFORMING ORGANIZATION NAME(S) AND ADDRESS(ES)

U.S. Army Engineer Research and Development Center (ERDC)
Cold Regions Research and Engineering Laboratory (CRREL)
72 Lyme Road
Hanover, NH 03755-1290

8. PERFORMING ORGANIZATION REPORT NUMBER

ERDC/CRREL TR-18-14

9. SPONSORING / MONITORING AGENCY NAME(S) AND ADDRESS(ES)

Assistant Secretary of the Army for Acquisition, Logistics, and Technology
103 Army Pentagon
Washington, DC 20314-1000

10. SPONSOR/MONITOR'S ACRONYM(S)

11. SPONSOR/MONITOR'S REPORT NUMBER(S)

12. DISTRIBUTION / AVAILABILITY STATEMENT

Approved for public release; distribution is unlimited.

13. SUPPLEMENTARY NOTES

ERDC 6.2 Geospatial Research and Engineering (GRE) ARTEMIS STO-R GRAIL

14. ABSTRACT

Connecting landforms to soil strength parameters can enable the prediction of soil bearing capacity and shear strength—important information for mobility and dust emission modeling. This project aimed to relate soil strength metrics to geomorphic landforms, focusing on five alluvial and aeolian landform classes in the Sonoran Desert. To achieve this, a variety of soil strength, dust emission, and soil texture measurements were made at 47 sites in California and Arizona; and these data were compared with landform classifications. Measurements of soil bearing capacity and shear strength varied significantly between landform classes. The aeolian landforms had significantly lower bearing capacity and shear strength than the alluvial landforms. The alluvial fan landform demonstrated consistently high soil strength, whereas the alluvial plain landform had relatively high mean soil strength but extreme site variability. The aeolian landforms were dominated by sand, whereas the alluvial landforms presented variable particle size distributions extending into loam and silt-loam classes. Silt and clay content were positively correlated with soil strength across all sites, while sand content was negatively correlated. Only the near-surface soil strength measures from the pocket penetrometer, Torvane, and vane shear correlated with dust emission flux and susceptibility.

15. SUBJECT TERMS

Geomorphology, Landforms, Remote sensing, Soils--Bearing capacity, Sonoran Desert--Soils

16. SECURITY CLASSIFICATION OF:			**17. LIMITATION OF ABSTRACT**	**18. NUMBER OF PAGES**	**19a. NAME OF RESPONSIBLE PERSON**
a. REPORT	**b. ABSTRACT**	**c. THIS PAGE**			**19b. TELEPHONE NUMBER** *(include area code)*
Unclassified	Unclassified	Unclassified	SAR	80	